2010

Growth Mechanism Of Titanium Nitride Nanowires And Their Physical, Structural And Biological Properties

Mainul Kader Faruque
North Carolina Agricultural & Technical State University

GROWTH MECHANISM OF TITANIUM NITRIDE NANOWIRES AND THEIR PHYSICAL, STRUCTURAL AND BIOLOGICAL PROPERTIES

by

Mainul Kader Faruque

A thesis submitted to the graduate faculty
in partial fulfillment of the requirements for the degree of
MASTER OF SCIENCE

Department: Mechanical Engineering
Major: Mechanical Engineering
Major Professor: Dr. Dhananjay Kumar

North Carolina A&T State University
Greensboro, North Carolina
2010

`

School of Graduate Studies
North Carolina Agricultural and Technical State University

This is to certify that the Master's Thesis of

Mainul Kader Faruque

has met the thesis requirements of
North Carolina Agricultural and Technical State University

Greensboro, North Carolina
2010

Approved by:

_____	_____
Dr. Dhananjay Kumar Major Professor	Dr. Jagannathan Sankar Committee Member
_____	_____
Dr. Devdas M. Pai Committee Member	Dr. Samuel P. Owusu-Ofori Department Chairperson

_____
Dr. Alan Letton
Interim Associate Vice Chancellor for Research and Dean of Graduate Studies

`

BIOGRAPHICAL SKETCH

Mainul Kader Faruque was born on July 10, 1983, in Dhaka, Bangladesh. He received his Bachelor of Science degree in Mechanical Engineering from Bangladesh University of Engineering and Technology (BUET) in November, 2006. He joined North Carolina Agricultural and Technical State University, Greensboro, in fall semester of 2008 for the Master's program in Mechanical Engineering. He is currently a candidate for the Master of Science degree in Mechanical Engineering.

`

ACKNOWLEDGMENTS

First of all, I want to express my warm gratitude to almighty god for everything I have achieved so far. Then I would like to thank my parents, family, and friends, whose love, work, and encouragement have made this endeavor possible. I would also like to express my sincere appreciation and my heartfelt gratitude to Dr. Dhananjay Kumar, advisor of my graduate studies, for the confidence, encouragement, guidance, and support throughout the study, and above all for his constructive criticism throughout the period of my research and graduate studies. I also wish to express my sincere thanks to Dr. Jagannathan Sankar and Dr. Devdas M. Pai for being a part of my thesis committee and for enlightening me with their knowledge.

My thanks also go to Dr. Xu, Dr. Yarmalenko, Dr. Yun, and Dr Ko. I am especially thankful to Dr. Waterman for her help and advice in biological measurements and analysis. I would also like to thank my colleagues in Dr. Kumar's research group for their heartiest cooperation throughout the completion of my master's degree. I also acknowledge the financial support from the National Science Foundation (NSF) and the Engineering Research Center (ERC) for Revolutionizing Metallic Biomaterials in the completion of my thesis.

`

TABLE OF CONTENTS

LIST OF FIGURES vii

LIST OF TABLES x

ABSTRACT xi

CHAPTER 1. INTRODUCTION 1

1.1 Nanowire 1

1.2 Properties of Nanowires 2

1.3 Applications of Nanowires 3

1.4 Thesis Objectives 7

CHAPTER 2. LITERATURE REVIEW 9

CHAPTER 3. EXPERIMENTAL METHODS 20

3.1 Pulsed Laser Deposition (PLD) 20

3.2 Scanning Electron Microscope (SEM) 23

3.3 Atomic Force Microscope (AFM) 25

3.4 X-ray Diffraction (XRD) 27

3.5 Electrochemical Corrosion Test 30

CHAPTER 4. RESULTS AND DISCUSSION 33

4.1 Substrates 33

4.1.1 Substrate selection 33

4.1.2 Substrate cleaning 34

4.1.3 Substrate surface modification by catalyst 34

4.2 Thin Film Deposition and Nanowire Fabrication 35
4.2.1 Growth rate measurement of gold and TiN films 35
4.2.2 Process to grow nanowires 35
4.3 Structural Properties 37
4.3.1 Effect of number of laser pulses on gold target in cluster formation 37
4.3.2 Effect of deposition temperature on TiN nanowire growth 39
4.3.3 Effect of background gas on TiN nanowire growth 43
4.3.4 Effect of number of laser pulses of TiN on nanowire length 45
4.3.5 Effect of substrate orientation on the vertical growth of nanowires 46
4.3.6 Tapering effect in nanowires 49
4.4 Corrosion and Biological Properties 54
4.4.1 Corrosion of nanowire 54
4.4.2 Cell culture 60
4.4.2.1 Objective 60
4.4.2.2 Aseptic technique 60
4.4.2.3 Accessories 61
4.4.2.4 Cell growth 62
4.4.2.5 Lactate dehydrogenase (LDH) release assay 63
CHAPTER 5. CONCLUSIONS AND FUTURE WORK 66
5.1 Conclusions 66
5.2 Future Work 67
REFERENCES 69

`

LIST OF FIGURES

FIGURES PAGE

1.1. Cross-section of nanowires 2

1.2. SEM images of Si nanowires (a) before and (b) after absorbing lithium..... 4

1.3. Titanium scaffolding with different pore size and bone tissue growth on the titanium scaffolding 6

1.4. (a) Individual mouse stem cell penetrated by silicon nanowires and (b) individual mouse stem cell grown on silicon nanowires 6

1.5. Crystal structure of TiN 8

2.1. The effect of gold thickness and deposition temperature on nanowire growth 10

2.2. Reduction of tapering of nanowire with O_2: Ar gas mixture ratios (a) 1:0, (b) 1:50, and (c) 1:100 11

2.3. The effect of mixture of gases on tapering of nanowire 12

2.4. The effect of temperature step in reduction of tapering (a) deposition at 340 °C and (b) started deposition at 340 °C (1 minute) then reduced to 295 °C (10 minutes) 14

2.5. Nanowires on different MgO substrate (a) (100), (b) (110), and (c) (111) 15

2.6. The effect of thermal annealing on structural quality and inter nanodots separation at (a) 300 °C, (b) 500 °C, and (c) 700 °C. Each pair represents a top-view (left) and cross sectional view (right) 17

2.7. SEM images of MgO films (a) without annealing, (b) 300 °C, (c) 500 °C, and (d) 700 °C 18

3.1. Schematic of pulsed laser deposition system 22

3.2. Schematic diagram of scanning electron microscope 24

3.3. Schematic of atomic force microscope 26

3.4. Diffraction of X-rays by planes of atoms 27

3.5. Two types of interference of waves (a) constructive and (b) destructive interference 28

3.6. Electrochemical corrosion testing setup 31

3.7. Plot of current density against potential 32

4.1. Crystal structure of MgO 33

4.2. Crystal structure of gold 35

4.3. Step by step procedure to grow TiN nanowires 36

4.4. SEM images of gold on MgO substrate with varying number of pulses (a) 50 pulses, (b) 100 pulses, and (c) 500 pulses 38

4.5. SEM images with varying deposition temperature (a) 400 °C, (b) 600 °C, and (c) 800 °C 40

4.6. Energy dispersive spectroscopy graph of TiN nanowires 41

4.7. SEM image to confirm the dependency of nanowire growth on gold 42

4.8. SEM image of TiN nanostructures grown in (a) vacuum, (b) argon, and (c) nitrogen environment 44

4.9. SEM images with varying number of pulses for TiN (a) 12,000, (b) 18,000, and (c) 30,000 pulses 45

4.10. SEM images of TiN nanowire on different orientation of substrate (a) MgO (100), (b) MgO (110), and (c) MgO (111) substrate 47

4.11. X-ray diffraction (XRD) θ-2θ scans of (a) MgO (100), (b) MgO (110), and (c) MgO (111) substrate 48

4.12. X-ray diffraction (XRD) θ-2θ scans of TiN nanowire on (a) MgO (100), (b) MgO (110), and (c) MgO (111) substrate 50

4.13. The effect of temperature for reducing tapering of TiN nanowire (a) entire deposition at 800 °C and (b) started deposition at 800 °C (3 minutes) then reduced to 600 °C (15 minutes) 52

4.14. The effect of time for reducing tapering of TiN nanowire by reducing the temperature to 600 °C after (a) 1 minute and (b) 3 minutes 53

4.15. X-ray diffraction (XRD) θ-2θ scans of TiN thin film on MgO (100) substrate 55

4.16. SEM images of (a) TiN thin film before corrosion test, (b) TiN thin film after corrosion test, (c) Mg substrate before corrosion test, and (d) Mg substrate after corrosion test 56

4.17. Potentiodynamic polarization curve of TiN thin film in (a) HBSS solution and (b) PBS solution 58

4.18. LDH release assay after (a) 4 hours and (b) 24 hours 65

`

LIST OF TABLES

TABLE PAGE

4.1. Corrosion potential and corrosion current data for TiN thin film and Mg substrate in HBSS solution 59

4.2. Corrosion potential and corrosion current data for TiN thin film and Mg substrate in PBS solution 59

`

ABSTRACT

Faruque, Mainul Kader. GROWTH MECHANISM OF TITANIUM NITRIDE NANOWIRES AND THEIR PHYSICAL, STRUCTURAL AND BIOLOGICAL PROPERTIES. **(Major Advisor: Dhananjay Kumar)**, North Carolina Agricultural and Technical State University.

Nanowires have attracted wide-spread attention from researchers around the world due to their enormous potential for basic studies and applications in materials and biological science and engineering. In this work, titanium nitride nanowires have been grown on a magnesium oxide substrate using a pulsed laser deposition technique. The selection of titanium nitride as a material of interest has been made due to its stellar properties of high melting point, good diffusion barrier, high hardness, good electrical conductivity, and scattered reports in the literature about its biocompatibility. In this work, gold has been used as a catalyst.

The most critical parameters for titanium nitride nanowire growth are the size of the gold catalyst and the substrate temperature. Before all the deposition experiments, thermal annealing of the substrate has been carried out, which affects the morphology of the final structures of titanium nitride nanowires. The morphology of the titanium nitride nanowires has been characterized by scanning electron microscopy. X-ray diffraction has been used to determine the crystalline structure and orientation of titanium nitride nanowires. The effect of substrate orientation, deposition temperature, and the nature and pressure of background gas on nanowire growth has also been examined in this study. The corrosion and biological behavior of titanium nitride nanowires investigated in this

study suggest that it is a biocompatible material and can safely be used in biological applications.

`

CHAPTER 1

INTRODUCTION

1.1 Nanowire

Nanowires are one-dimensional nanostructures. They are usually fabricated using vapor-liquid-solid (VLS) method [1]. The synthesis of one dimensional (1D) structure like nanowires and nanobelts has attracted more focus in biological, electronic, and photonic field in recent times because of their stellar properties [2]. The reduction of size of the crystalline structure improves the properties of the material as a whole [3]. According to the principle of the classical VLS mechanism, the shape of the nanowires can be determined by the catalyst droplet size. The other parameters that also influence the nanowire growth are substrate temperature, ambience pressure, substrate surface orientation etc. In this research, we have focused our studies on the effect of droplet size of the catalyst and the deposition temperature on the growth of titanium nitride (TiN) nanowires. A wide number of research groups have reported the synthesis of TiN films using either TiN targets [4] or using TiN in nitrogen (N_2) environment [5]. Nanowires of other materials that have shown promise in various applications include metals (Al, Si) [6], metal nitrides (TiN, GaN) [7], carbides (SiC) [8] and oxides (ZnO, MgO) [9].

There are two common approaches of synthesizing nanowires; the top-down and the bottom-up method [10]. In a top-down approach, a bulk material is cut down into tiny pieces through different methods such as lithography and electrophoresis. On the other

`

hand, in a bottom-up approach, nanowires are fabricated by the combination of constituent's ad-atoms. Most nanowire fabrication techniques are based on a bottom-up approach. The cross-sectional shape of nanowires can be rectangular, hexagonal, cylindrical, and triangular as shown in Figure 1.1.

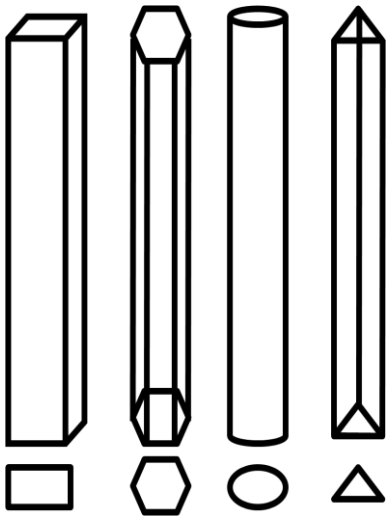

Figure 1.1. Cross-section of nanowires

1.2 Properties of Nanowires

Nanowires exhibit many interesting properties different from the corresponding bulk or three dimensional (3-D) materials. The reason is that, electrons located in the nanowires are normally quantum-confined laterally. So, these nanowires occupy energy levels which are dissimilar from the conventional continuum of energy levels observed in a bulk material [11]. Depending upon the material, a nanowire can show the properties of an insulator, a semiconductor or a metal. Insulators do not carry charge, whereas metals

`

carry electric charges. Semiconductors fall in between these two. Semiconductors can transport a charge under perfect conditions. By suitably arranging semiconductor wires, it is possible to make transistors, which can be used as switches or amplifiers [12].

At the nanoscale, elements show some different properties than normally anticipated. For example, gold (Au) has a melting point of 1,064 °C when it is in bulk form. But this melting point can change for gold if it is in nanoparticle form [13]. Also at the nanoscale, gold behaves like a semiconductor, whereas it is a conductor in bulk form. Again, in bulk, aluminum is not magnetic, but a nanopaticle of aluminum is magnetic. This property difference is because when any bulk material is reduced to nanoscale, there is a significant increase in the surface-to-volume ratio and the atoms sitting on the surfaces take on an overwhelming significance in determining the properties of the object as a whole.

Another exciting property is that certain nanowires are ballistic conductors [12]. In conventional conductors, electrons interact with the lattice vibrating at its equilibrium position in the material. This reduces the speed of the electrons and forms heat as a byproduct. But in ballistic conductors, the electrons can move through the conductor without any collision with atoms. As a result, nanowires can conduct electricity efficiently without substantial dissipation of electrical energy into heat energy.

1.3 Applications of Nanowires

By using silicon nanowires, some researchers from Stanford University have created a rechargeable lithium-ion battery. This battery has the ability to power laptops,

`

iPods, video cameras, cell phones, and numerous other devices [14]. These silicon nanowires have the ability to absorb lithium as shown in Figure 1.2 [15], so this can be used as a capacitor to store energy. This new lithium ion battery, have fabricated by Yi Cui and his research group can generate ten times more electricity than conventional lithium-ion batteries. A laptop that now operates on battery for two hours can be operated for twenty hours, which can be great use to long distance based business travelers.

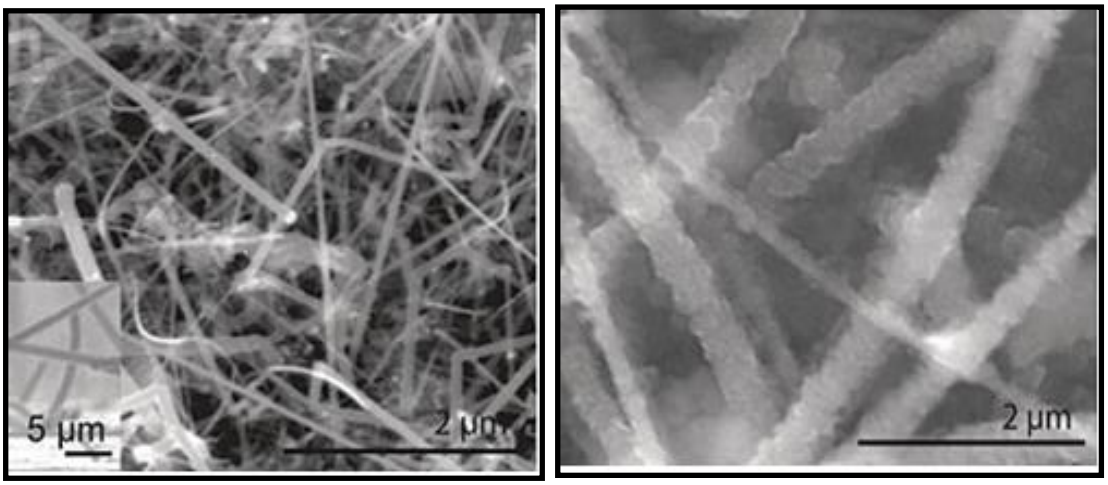

(a) (b)

Figure 1.2. SEM images of Si nanowires (a) before and (b) after absorbing lithium [15]

Most nanowires are very good conductors or semiconductors, so it is possible to make transistors out of these nanowires. Their trifling size makes it feasible to place more transistors than before in a single microprocessor, which can expedite the function and reduce power consumption. As a result, the speed of the computer will progress dramatically [12]. In the future, nanowires can be used to link infinitesimal components

in extremely small circuits [12]. Nanowires usually appear in packages. So these can be used as triboligical additives to augment the friction characteristics of electronic transducers and actuators. Because of their high surface-to-volume ratio, nanowires are also exclusively apposite for dielectrophoretic manipulation. The key step to generate dynamic electronic elements is to chemically dope a semiconductor nanowire. This has already been conducted in individual nanowires to create p-type and n-type semiconductors [16-18]. Nanowires can also be used as a mass sensor to measure the mass of very small particles [19]. Researchers from University of Arkansas have used titanium oxide nanowires to coat titanium implants as shown in Figure 1.3 [11]. They have found that muscle tissue sometimes does not stick well to titanium implants. But when the implant is coated with titanium oxide nanowires, the tissue can bind to the implant resolutely. This reduces the possibility of implant failure [11].

Researchers from the Gladstone Institute of Cardiovascular Disease have performed research with nanowires and stem cells [20]. They have supplied an electric current through a nanowire into the stem cell to investigate the process of cell differentiation. They have fabricated a technique to introduce silicon nanowires in living cells, as shown in Figure 1.4 [20]. This technique helps them to connect cells with one another. Nanowires have been connected with external source and sensors, which have the potential to conduct genetic material to explicit organelles in a cell. Nanowires have application in the chemical field too. Some researchers have created a molecular sensor using silicon nanowires [21].

`

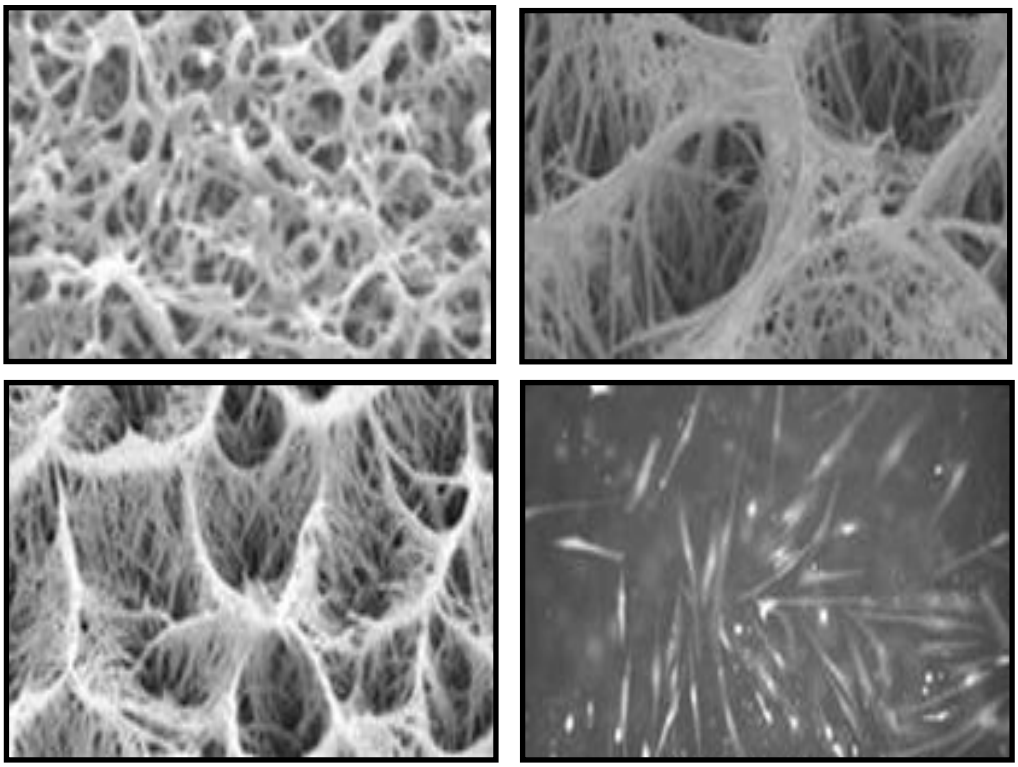

Figure 1.3. Titanium scaffolding with different pore size and bone tissue growth on the titanium scaffolding [11]

(a) (b)

Figure 1.4. (a) Individual mouse stem cell penetrated by silicon nanowires and (b) individual mouse stem cell grown on silicon nanowires [20]

`

1.4 Thesis Objectives

The current thesis has focused on mastering the fabrication, developing a fundamental understanding of titanium nitride (TiN) nanowires, and exploring their applications in electronic and biological devices. TiN possesses a combination of excellent properties like high quality hardness, electrical conductivity, corrosion resistance, and diffusion barrier [22] (used between two metals to protect one from corrupting the other). TiN can also be used as a hard thin film coating, to enhance the hardness of metals, alloys and ceramics, and as a binder in plastics and polymers. Another important feature of TiN is that these coatings are free from any sort of thermal irritation, acute systemic toxicity or cytotoxicity [23].

Some of its common parameters includes; color: yellow brown, melting point: 3290 °C, lattice constant: 4.24 Å, lattice structure: face centered cubic (FCC), compressive strength: 0.9724 GPa, element: Ti (77%) and N (23%).Titanium is widely being used as an effective implant material. But titanium creates problems in a particular surface of total joint implants [24, 25]. The use of TiN coating on titanium implant can resolve this limitation by increasing surface hardness [26, 27]. An implant coated with TiN exhibits decrease in metal wear and corrosion compared to other implants [28, 29]. TiN has significant use in biomedical applications as dental prostheses, and as a coating for cardiovascular and orthopedic implants [30, 31]. It is also found that titanium or aluminum implants coated with TiN can enhance cell adhesion or proliferation [32]. TiN can also be used as a diffusion barrier in orthopedic prosthesis and cardiac valves due to increased hemocompatibility and surface characteristics [33].

`

TiN possesses very good corrosion and wear resistance. So it can be widely used as a primal material as protective coating to improve the surface properties of different metals [34, 35]. TiN can also be used as a hardener and protector for cutting and sliding surfaces. Its golden appearance makes TiN suitable for using in decorative purposes and as a non-toxic exterior for medical implants. It can also used as a diffusion barrier in the microelectronics industry [35, 36]. TiN has another interesting property. If the thin film of titanium nitride is cooled down to absolute zero, TiN acts as a super insulator. During the process, resistance is increased by a factor of 100,000 [37]. Due to these outstanding properties and applications, TiN has enormous use in the electrical, mechanical, and biological industry, which strongly motivated us to work with this material. Figure 1.5 represents the cubic structure of TiN.

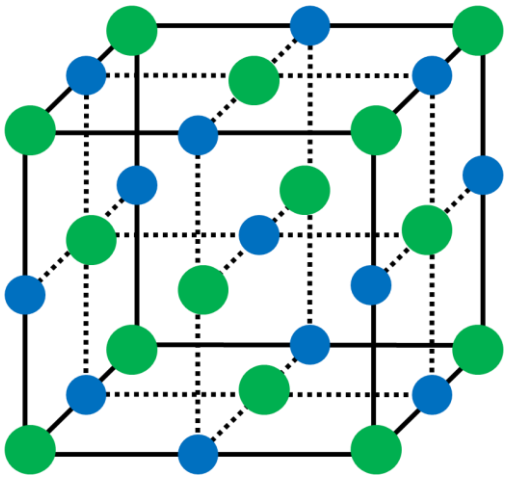

Figure 1.5. Crystal structure of TiN

`

CHAPTER 2

LITERATURE REVIEW

Due to their enormous applications nanowires have become an interesting topic for researchers around the world. Yanagida et al. [38] from Osaka University have grown magnesium oxide (MgO) nanowires using the pulsed laser deposition technique. MgO is very commonly used as a single crystal substrate for thin film growth. It can also be used as catalysis, additives in refractory etc. In this paper, they have described the effect of gold size and substrate temperature on MgO nanowire growth. It is found that both these parameters have a strong influence on nanowire formation, as shown in Figure 2.1 [38]. In this figure, region A indicates the nanowire growth, in region B there is an initiation of nanowire growth and in region C there is no nanowire at all. Thus, the finding of this study emphasizes the need of optimization of gold nanodots size and deposition temperature for the growth of good quality nanowire. It can also be noticed that when the growth temperature decreases, the threshold thickness (size) of gold film (nanodots) also decreases. The critical thickness/size for a stable gold film or a gold nanodots has been attributed primarily to the lowering of the melting temperature of gold with reduction in its thickness (or size) [39]. It has been shown by Yanagida et al. [38] that for nanowire growth, the critical temperature should be in the range of 450-900 °C and the critical thickness of gold nanodots should be in the range of 1-5 nm.

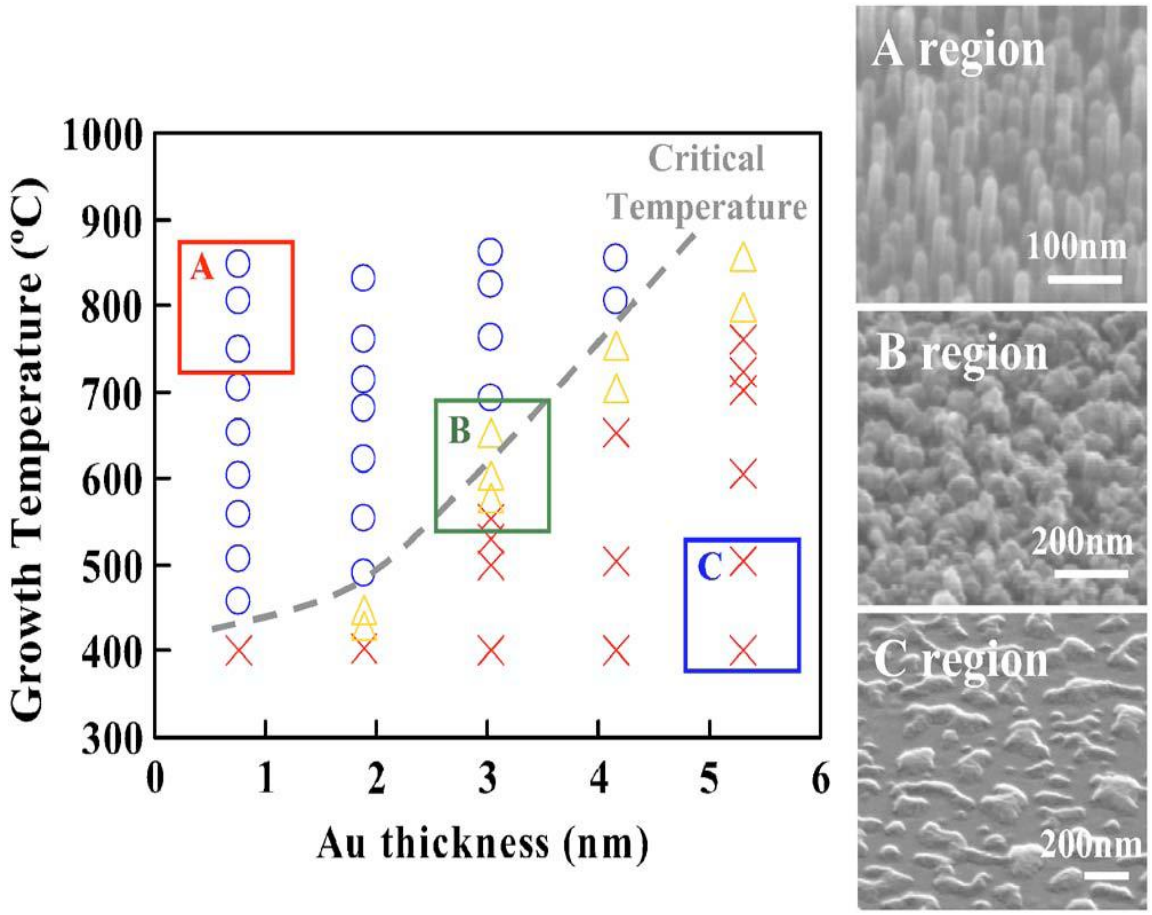

Figure 2.1. The effect of gold thickness and deposition temperature on nanowire growth [38]

`

It is also important that the diameter of the nanowires be uniform throughout its length [40]. Non-uniformity in the diameter of nanowires arises because of tapering effect. Tapering occurs when the catalyst diffuses from the tip. Nagashima et al. [40] have reported the way of reducing the tapering effect in nanowires. To overcome this problem, they have used a mixture of oxygen (O_2) and argon (Ar) with varying oxygen partial pressure. This method helps to suppress the catalyst diffusion from the tip. Figure 2.2 [40] shows the scanning electron microscope (SEM) images of MgO nanowires and how the tapering can be reduced with varying mixed gas ratio. It is clearly seen from the figure that the tapering is reduced as the ratio of Ar increases in the mixture of O_2 and Ar. Figure 2.3 [40] shows the quantitative variation of the degree of tapering and tip diameter with O_2: Ar gas ratio. It is interesting to note from this figure that while the degree of tapering reduces, the tip diameters of all the nanowires remain constant with varying mixed gas ratio.

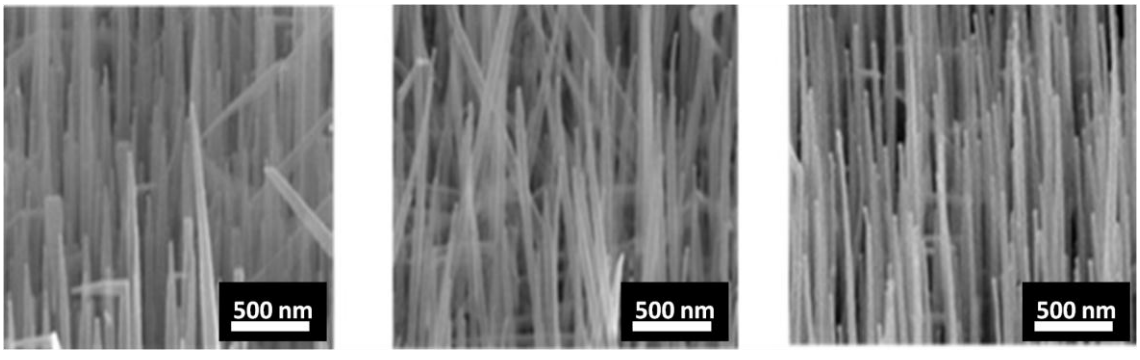

(a) (b) (c)

Figure 2.2. Reduction of tapering of nanowire with O_2: Ar gas mixture ratios (a) 1:0, (b) 1:50, and (c) 1:100 [40]

`

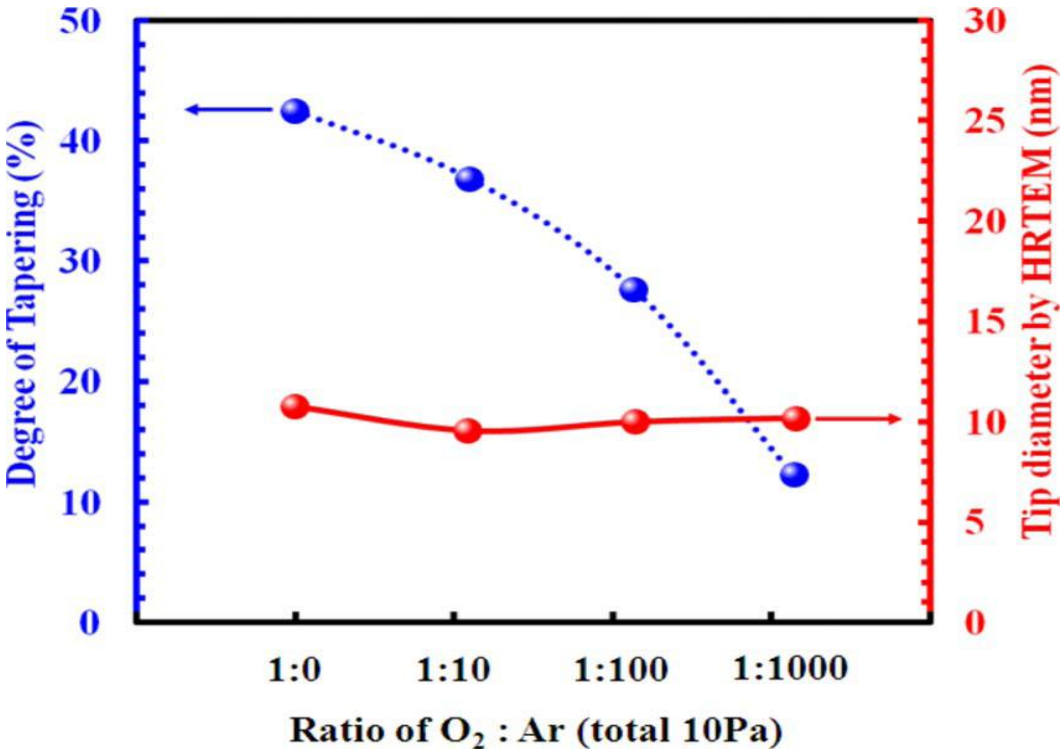

Figure 2.3. The effect of mixture of gases on tapering of nanowire [40]

Jagannathan et al. [41] have established another way to reduce tapering in nanowires. Their studies have shown that the deposition temperature can play either an adverse or a beneficial effect on tapering, depending on the deposition temperature. It is very important to reduce the tapering from the nanowire. At the tapered side there is a possibility of stress development, which might lead to nanowire failure. According to Jagannathan et al. [41], higher temperatures are needed for the growth of structurally sound quality nanowires with longer lengths. But at high temperature, there is a possibility of sidewall oxidation of nanowires. This sidewall oxidation can be significantly reduced at lower temperatures. So, low temperature deposition can reduce the tapering effect from nanowires. However, lower temperatures reduce the nucleation

density of nanowire, which in turn, results in poor growth of nanowires or sometimes even the formation of continuous thin films instead of nanowires [42]. So there is a conflict in the deposition temperature required for non-tapered nanowire growth. To overcome these conflicting effects of deposition temperature, two-stage deposition process is used for the growth of good quality nanowires. For example, the first stage of Germanium (Ge) nanowires growth involves the depositing nanowires at higher temperatures (340 °C) that are followed (second stage) by continued growth of nanowires at reduced temperature (295 °C). An advantage of a two stage process for nanowire formation without tapering is illustrated in Figure 2.4 [41]. It can be clearly seen from the figure that single-stage deposition at 340 °C does exhibit some tapering effect of the nanowire ends. But when a two-stage deposition technique is used, the tapering of the nanowires reduces as shown in Figure 2.4 (b).

The orientation of the substrate has a strong effect on the growth direction of the nanowires. It is found that the orientation of substrate has a significant impact on the physical, optical, and electrical properties of the deposited film. Nagashima et al. [43] have discussed the dependency of growth direction of magnesium oxide (MgO) nanowires on substrate orientation. They have deposited MgO nanowires on three different MgO substrates such as MgO (100), MgO (110), and MgO (111) to see the effect of substrate orientation, as shown in Figure 2.5 [43]. These images indicate that MgO nanowires grow vertically only on MgO (100) substrate. On the other two substrates, the nanowires grow randomly in different directions. The growth direction of nanowires can be controlled by changing the orientation of substrate.

`

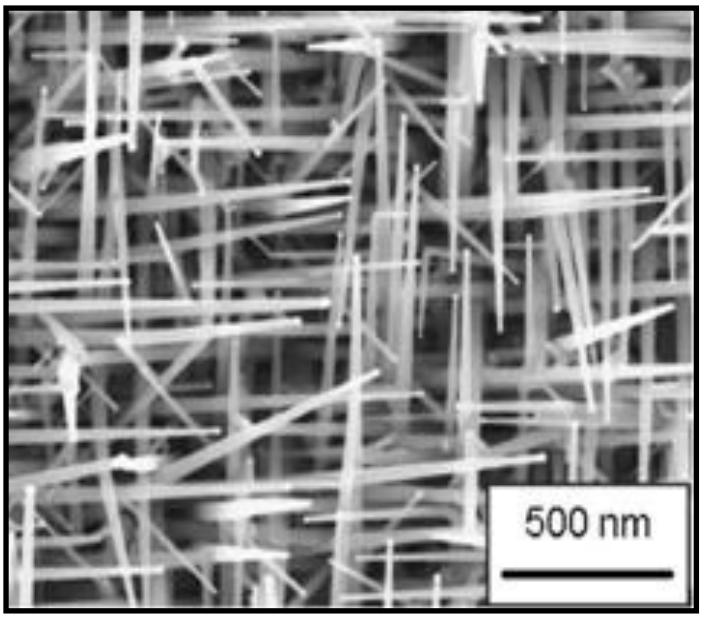

(a)

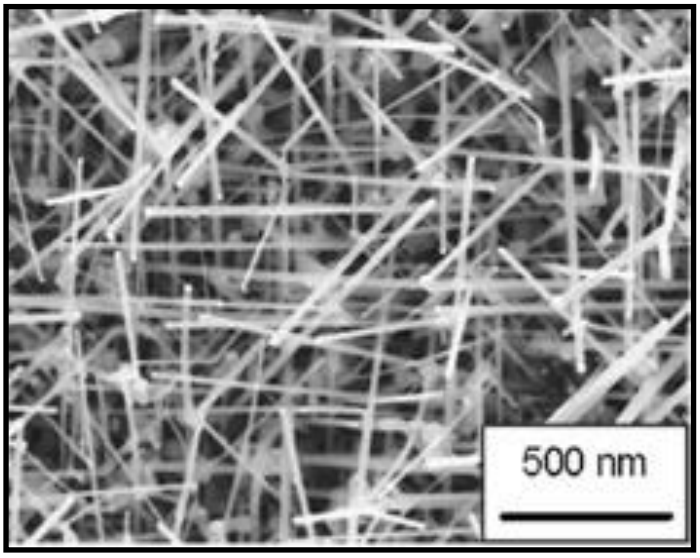

(b)

Figure 2.4. The effect of temperature step in reduction of tapering (a) deposition at 340 °C and (b) started deposition at 340 °C (1 minute) then reduced to 295 °C (10 minutes) [41]

`

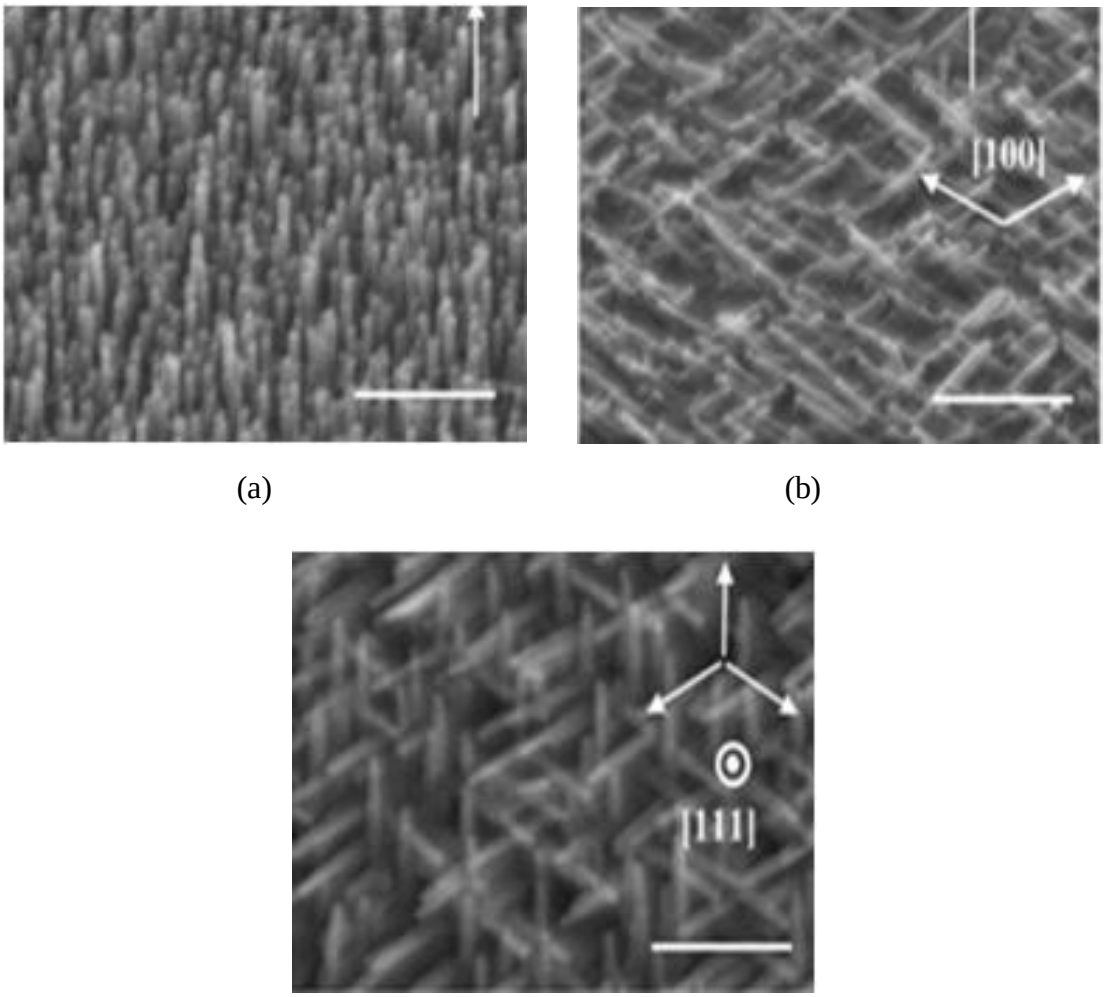

(a) (b)

(c)

Figure 2.5. Nanowires on different MgO substrate (a) (100), (b) (110), and (c) (111) [43]

`

The annealing of substrates covered with gold nanodots also plays an important role in the growth of nanowires. Kim et al. [42] have investigated the effect of thermal annealing of the gold coated substrates before the nanowire growth. First of all they have deposited gold layer of about 3 nm thick on the silicon wafer. After that they have heated the gold coated substrate prior to MgO deposition at different temperatures such as 300, 500, and 700 °C for 30 minutes to study the effect of annealing temperature. During the deposition nitrogen (N_2) has been used as a background gas.

It is clearly seen in Figure 2.6 [42] that gold dots on substrates annealed at 700 °C are more crystalline in nature and have larger separation from each other than those substrates annealed at 300 °C or even 500 °C. As seen in Figure 2.6, the annealing of gold films at lower temperatures (viz. 300 and 500 °C) does not promote cluster formation and the gold remains in a film form, making them unsuitable candidates for nanowire growth purposes. But at high temperature (700 °C), well distinctive gold cluster can be observed which facilitates MgO nanowire growth on the silicon (Si) substrate. Evidence in favor of this argument is presented in Figure 2.7 [42]. Here MgO is in the form of a continuous film as the gold coated substrate is not annealed [Figure 2.7 (a)], MgO begins to form in rod-like structures scattered throughout the substrate, when they are annealed at low temperatures such as 300 and 500 °C [Figure 2.7 (b) and (c)], and finally a distinct growth of MgO nanowires is observed on the substrate annealed at 700 °C [Figure 2.7 (d)]. So high temperature annealing is very vital for fabricating gold cluster which in turn results in good quality nanowires.

`

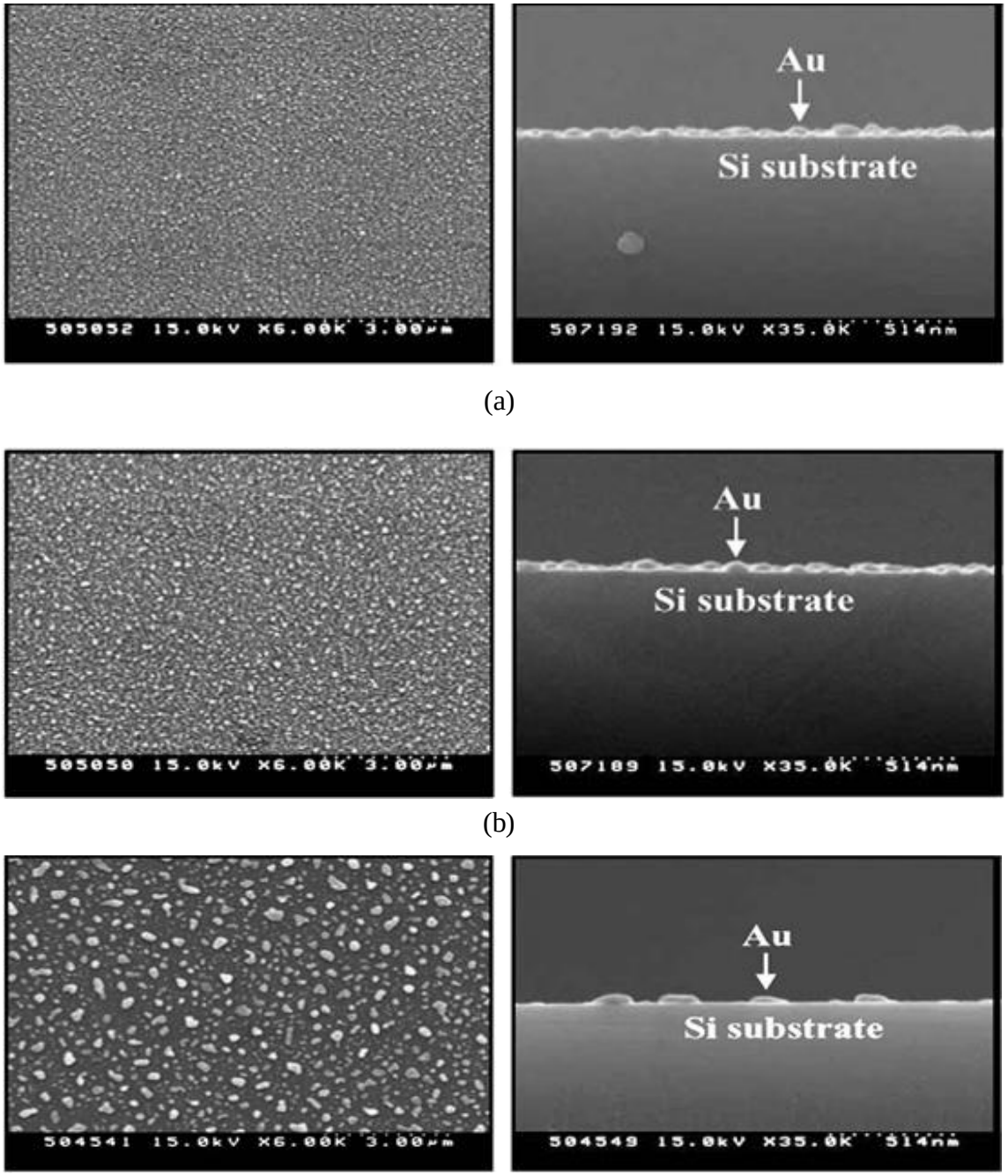

Figure 2.6. The effect of thermal annealing on structural quality and inter nanodots separation at (a) 300 °C, (b) 500 °C, and (c) 700 °C. Each pair represents a top-view (left) and cross sectional view (right) [42]

`

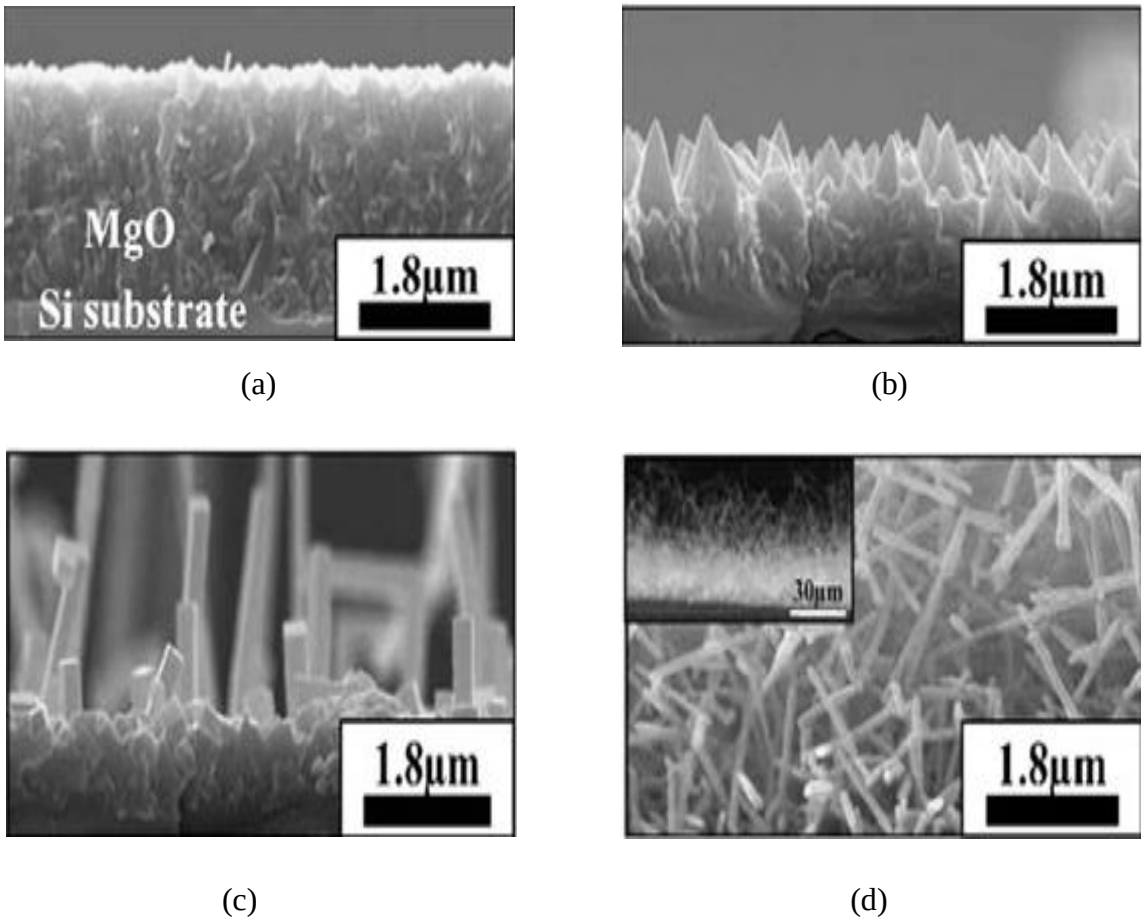

Figure 2.7. SEM images of MgO films (a) without annealing, (b) 300 °C, (c) 500 °C, and (d) 700 °C [42]

In conclusion, it is clear that a lot of research is going on into nanostructures especially nanowires, because of their outstanding properties and stellar applications. Although some of the properties and mechanisms of nanowire formation are still vague, the rapid growth of this field is indisputable. This has inspired us to work in this field. We have grown TiN nanowires on MgO substrate with different orientations and have characterized them using a wide variety of characterization tools such as scanning electron microscope (SEM), X-ray diffraction (XRD), atomic force microscope (AFM),

`

profilometer etc. We have also examined the corrosion and biological characteristics of these nanowires to explore their application as a coating material on regularly-used implant materials in the human body.

`

CHAPTER 3

EXPERIMENTAL METHODS

3.1 Pulsed Laser Deposition (PLD)

There are numerous techniques for growing nanostructures that include chemical vapor deposition [44], physical vapor deposition [45], sol gel process [46] etc. Pulsed laser deposition (PLD) is a physical vapor deposition technique which has been using successfully for depositing high quality thin film for more than twenty years. The method has been using very commonly for fabrication of nanostructures. The basic PLD system includes a laser source, a vacuum chamber with target and substrate holder, and a set of optical elements such as mirrors, lenses, and apertures. In PLD, a high-power laser beam is used to melt, evaporate and ionize the target material located inside a vacuum chamber. When the laser beam hits the target material, this laser energy first converted to an electrical energy and then into thermal, chemical and mechanical energy. This results in evaporation, ablation, and plasma formation from the target. All this process takes place within 30 ns. The thickness of the material evaporated is given by,

$$d = \frac{5.84X10^{-2}}{\rho} \times \left(M/T_B\right)^{1/2} \times P_e \quad (1)$$

where

d = thickness of material evaporated

ρ = density

M = molecular weight of the target material

`

T_B = boiling point

P_e = atmospheric pressure

The film forming atoms or molecules impinge on the substrate with a dimension known as the radius of the cluster is given by,

$$r^* = \frac{-2(a_1\gamma_{fv}+a_2\gamma_{fs}-a_2\gamma_{sv})}{a_3\Delta G_v} \quad (2)$$

where

r* = radius of cluster

a_1, a_2, and a_3 = geometric constant

γ_{fv} = interfacial energy between film and vapor

γ_{fs} = interfacial energy between film and substrate

γ_{sv} = interfacial energy between substrate and vapor

ΔG_v = change in Gibbs free energy

This vaporized material, containing ions, electrons, neutrals, molecules, atoms etc., is known as a laser-produced plasma plume. This plume is extremely directional and its contents move towards the substrate where they condense to form a film. In a PLD system, the laser power energy, the spot size, and the frequency are important factors that influence the quality of film growth. To reduce the surface defects and to avoid particulate formation, the laser fluence should be kept slightly above the ablation threshold. The schematic of a pulsed laser deposition (PLD) system is shown in Figure 3.1. In a PLD, the deposition can be carried out either in ultra high vacuum or in the presence of a background gas, such as oxygen, argon, nitrogen etc. The background gases are introduced to promote surface reaction or to maintain film stoichiometry.

`

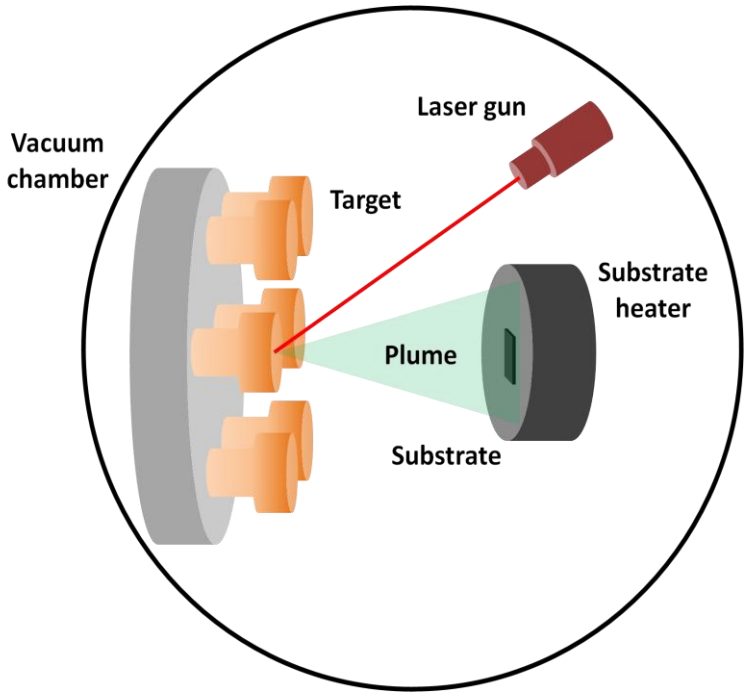

Figure 3.1. Schematic of pulsed laser deposition system

PLD is a simple process. It is very cost effective as one laser can serve many vacuum systems. PLD is a fast process too. In PLD, multiple targets can be mounted, which can enable one to deposit multilayer films of different materials without breaking the vacuum. The popularity of PLD had grown immensely high after the fabrication of very good quality high temperature superconducting $YBa_2Cu_3O_{7-d}$ thin films using this method in 1987. Soon after that, high temperature superconductivity in cuprates was discovered by Bednorz and Muller for which they were awarded the Nobel Prize for Physics in 1986 [47]. After that time, a lot of materials that are usually difficult to deposit using other techniques, have been successfully deposited by PLD. The applications of these PLD generated materials vary from the construction of superconducting and

`

insulating circuit components to enhanced wear and biocompatibility for medical applications. In PLD, the plume is highly directed, so it is hard to get a uniform deposition. This deficiency can be reduced by rastering and rotating the target surface during deposition. PLD can also lead to splashing or deposition of particulates on the film. There are some ways to resolve this problem; by using a high velocity pass filter, and using a high density and smooth target with regular polishing of the target before each deposition [48].

3.2 Scanning Electron Microscope (SEM)

Scanning electron microscope (SEM) is useful to produce high-resolution micro structural images of materials. It can also be used to identify phase and crystal structure of materials. An optical microscope creates a magnified image using light waves by a series of glass lenses. A scanning electron microscope uses an electron beam instead of a light source to form an image. An SEM can create very comprehensive three-dimensional images with very high resolution compared to a conventional light microscope. The blending of better resolution, higher magnification, greater depth of focus, and easy sample preparation makes an SEM the most commonly used device in the research arena today.

In an SEM, a high quality electron beam emits from an electron gun located at the top. The electron beam passes through objective and condenser lenses that focus the electrons to a very fine spot on the sample. A set of scanning coils located at the bottom is then energized by a scan generator. It creates a magnetic field which rasters the beam

across the specimen. When the beam strikes the sample surface, secondary electrons come out of the sample. These electrons are then gathered by a detector, where these are converted to signals. Detector sends these signals to a screen to create the final image. The schematic of an SEM is illustrated in Figure 3.2.

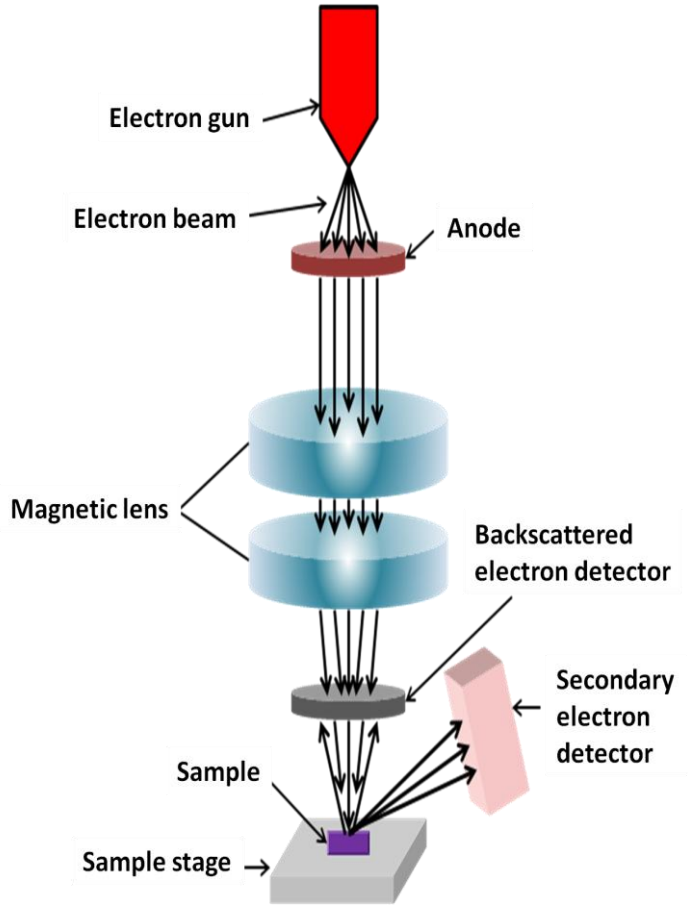

Figure 3.2. Schematic diagram of scanning electron microscope

`

3.3 Atomic Force Microscope (AFM)

The limitation of a scanning electron microscope (SEM) is that the sample needs to be conducting or semiconducting to create an image. This limitation can be overcome by using an atomic force microscope (AFM) which can be used to analyze non-conducting materials. In an AFM, any sort of sample, including polymers, ceramics, glass, biological samples, composites etc., can be examined. AFM can characterize samples at the microscopic level and produce three-dimensional images. The resolution of an AFM in the x-y direction varies from 0.1 to 1.0 nm and in the z direction is about 0.01 nm. In AFM, a vacuum environment is not essential. Due to these stellar features, AFM has made a massive impact in the fields of material science, chemistry, biology, physics etc.

AFM consists of a cantilever beam with a sharp tip at the end of the cantilever. The tip is normally made of silicon or silicon nitride. The radius of curvature of these tips varies from 1-20 nm. In AFM, a fine sharp tip is scanned over the sample surface. As the tip is resisted or magnetized by the surface of the sample, the cantilever beam deflects. A laser spot reflected from the top surface of the cantilever is used to measure the amount of deflection of the cantilever. Graph of this deflection versus tip position on the surface of the sample results in a topographical map of the surface.

AFM operates in three different modes which include contact mode, non contact mode, and the tapping mode. Contact mode is also known as the static mode. In the contact mode, deflection of the cantilever is directly used to measure the topography of the surface by dragging the cantilever across the surface of the sample. In a non-contact

and tapping mode, also known as dynamic mode, an external source is used to oscillate the cantilever. By detecting the changes to the resonant frequency or the amplitude of the cantilever, the sample can be characterized. Figure 3.3 shows the operating principle of atomic force microscopy.

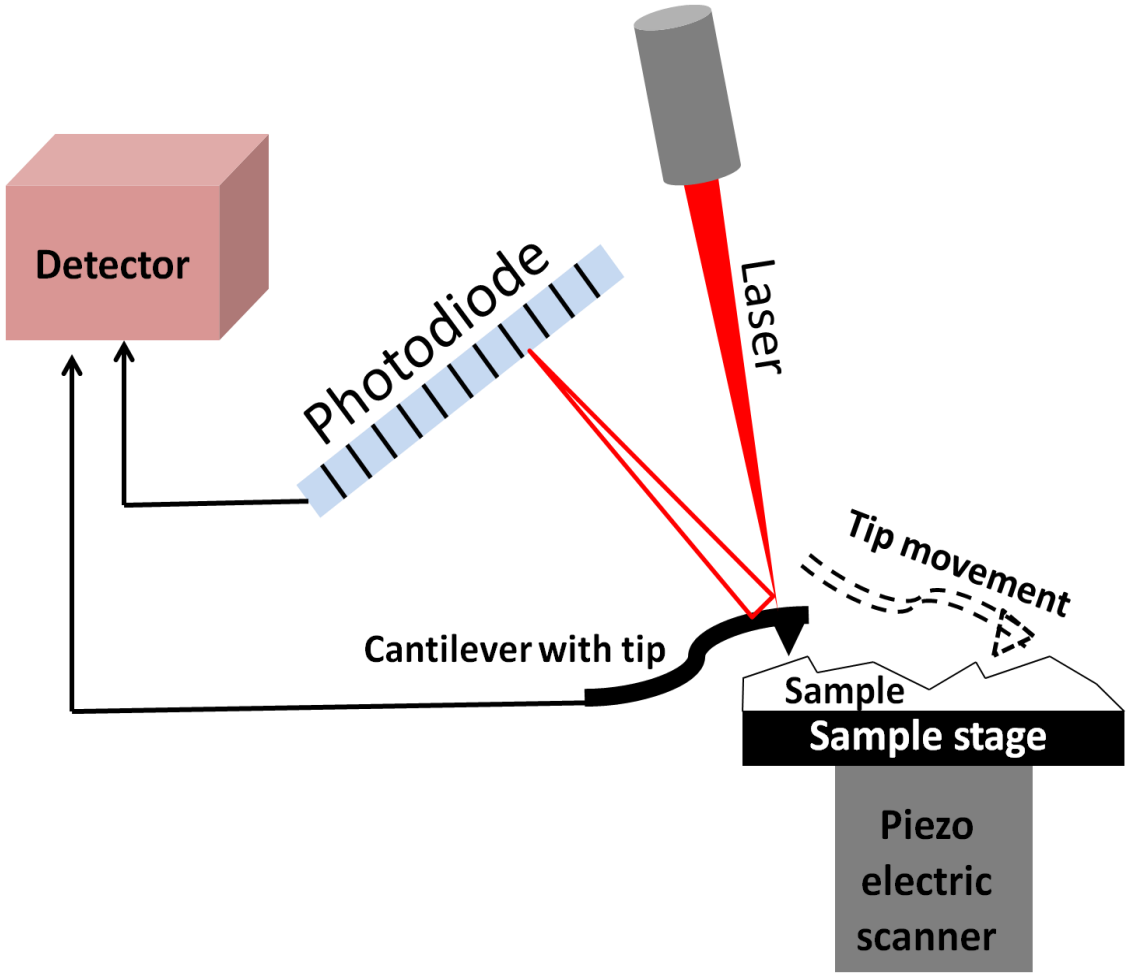

Figure 3.3. Schematic of atomic force microscope

`

3.4 X-ray Diffraction (XRD)

A solid material can be crystalline or amorphous. In a crystalline solid, the atoms are arranged in a regular manner, whereas in amorphous solid atoms are arranged in random way. Approximately 95 % of solid materials can be classified as crystalline. X-ray diffraction (XRD) method is routinely used as a finger-print method for the characterization of solid materials. XRD is a non-destructive method to determine the average spacing between atoms, to measure the thickness of thin films and multilayers, to find the crystal structure and orientation of material, to determine the size, shape, strain, grain size, epitaxy etc. X-ray is an electromagnetic radiation, with wavelength ranging between 0.01-10 nm. When a beam of X-rays hits on a solid material, a part of the beam is spread in all directions by electrons linked with each atom, and produces a diffracted beam as shown in Figure 3.4.

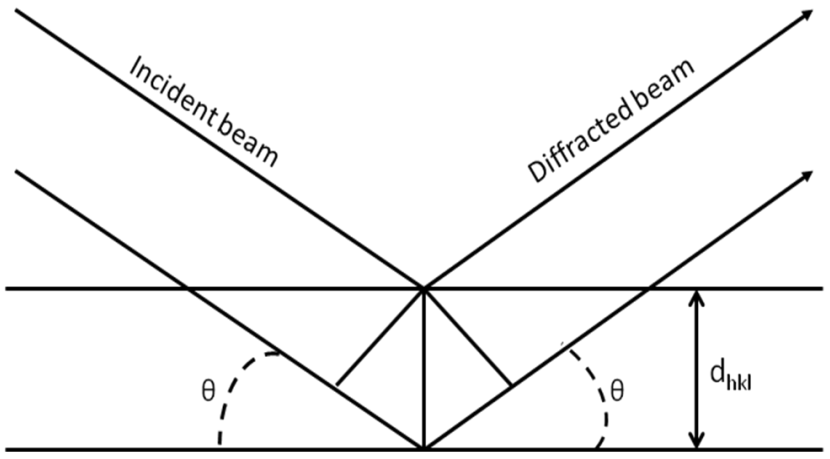

Figure 3.4. Diffraction of X-rays by planes of atoms

`

These scattered beams from the crystal lattice follow two conditions. The angle of incidence is equal to the angle of scattering and the path length difference is identical to an integer number of wavelengths. There are two types of interference. If the waves are moving in phase with one another, constructive interference will occur. If the waves are out of phase with one another, destructive interference will occur. For getting a diffraction pattern, the waves must constructively interfere. Figure 3.5 shows the constructive and destructive interference.

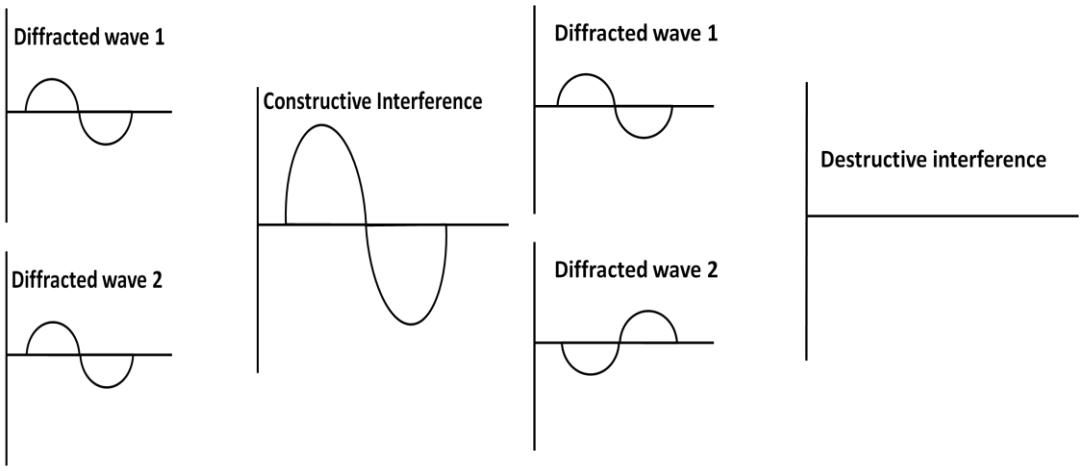

Figure 3.5. Two types of interference of waves (a) constructive and (b) destructive interference

English physicists Sir W. H. Bragg and his son, Sir W. L. Bragg, developed a relationship between the X-ray wavelength, interatomic distance and diffraction angle known as Bragg's law. According to this law,

$$n\lambda = 2d_{hkl}\sin\theta \quad (3)$$

`

where

n = order of reflection

λ = wavelength of the impinging X-ray beam

d_{hkl} = distance between atomic layers of a crystal

θ = angle of incident

d_{hkl} is a function of miller indices (h, k, and l) and given by,

$$d_{hkl} = a / \sqrt{(h^2+k^2+l^2)} \quad (4)$$

where

a = lattice parameter

The thickness of a thin film can be calculated using Scherer's formula is given by,

$$t = K\lambda / (B\cos\theta) \quad (5)$$

where

t = thickness of the film

K = Scherer's constant

B = full width at half maximum

θ = Bragg's angle

In the X-ray diffraction (XRD) technique, inter planar spacing of a crystal is used for characterization purposes. During an XRD experiment, the wavelength of the incident X-ray is known. The incident angle can be determined from the experiment. So the d-spacing between the crystal lattice planes can be calculated by solving Bragg's equation which gives us information about the crystal structure of the material.

`

3.5 Electrochemical Corrosion Test

The study of corrosion improves the understanding of the mechanism and reasons for corrosion, which helps one to prevent it from occurring. Corrosion can be described as the destruction of metal due to a reaction with the environment. Normally, it begins at the surface and occurs in the presence of moisture. For metals, the corrosion procedure is commonly electrochemical, which means a chemical reaction where there is a transfer of electrons from one chemical to other. A reaction where metals lose electrons is called an oxidation reaction. It takes place at the anode side. For example:

$$Fe \qquad Fe^{2+} + 2e^{-} \tag{6}$$

On the other side, the process of gaining an electron during the reaction termed as reduction. It occurs at the cathode. Reduction is sometimes called as cathodic reaction. For example:

$$2H^{+} + 2e^{-} \qquad H_2 \tag{7}$$

So, a complete electrochemical reaction will be the sum of an oxidation and a reduction reaction. The total rate of oxidation must equal to total rate of reduction. To measure the corrosion, we need a setup consisting of a reference and a counter electrode, an electrolyte solution, and the sample which is also known as working electrode. The setup is shown in Figure 3.6. All the electrodes are connected to a potentiostat and placed in the electrolyte solution. Then a voltage is applied to the electrodes. In this process, the applied potential is increased with time and the corresponding current is measured. From the energy difference between working and reference electrode, the corrosion potential is measured.

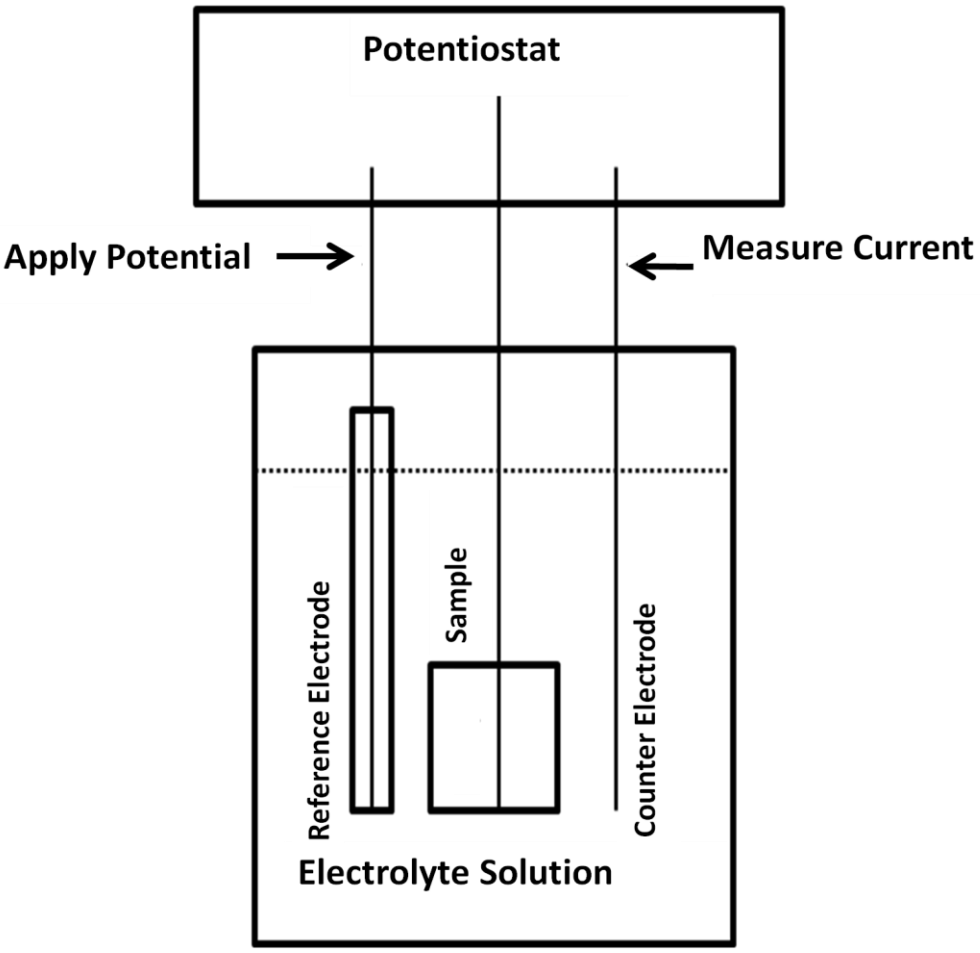

Figure 3.6. Electrochemical corrosion testing setup

`

Then the current density is plotted against the potential as shown in Figure 3.7. In this figure, the horizontal axis is the current density on the logarithmic scale and vertical axis represents the potential. The curved line represents the total current (anodic and cathodic). The intersection of the slope of the cathodic and anodic current gives the corrosion potential (E_{corr}) and corrosion current (I_{corr}). Lower I_{corr} corresponds to a higher corrosion resistance and higher E_{corr} means a higher corrosion resistance.

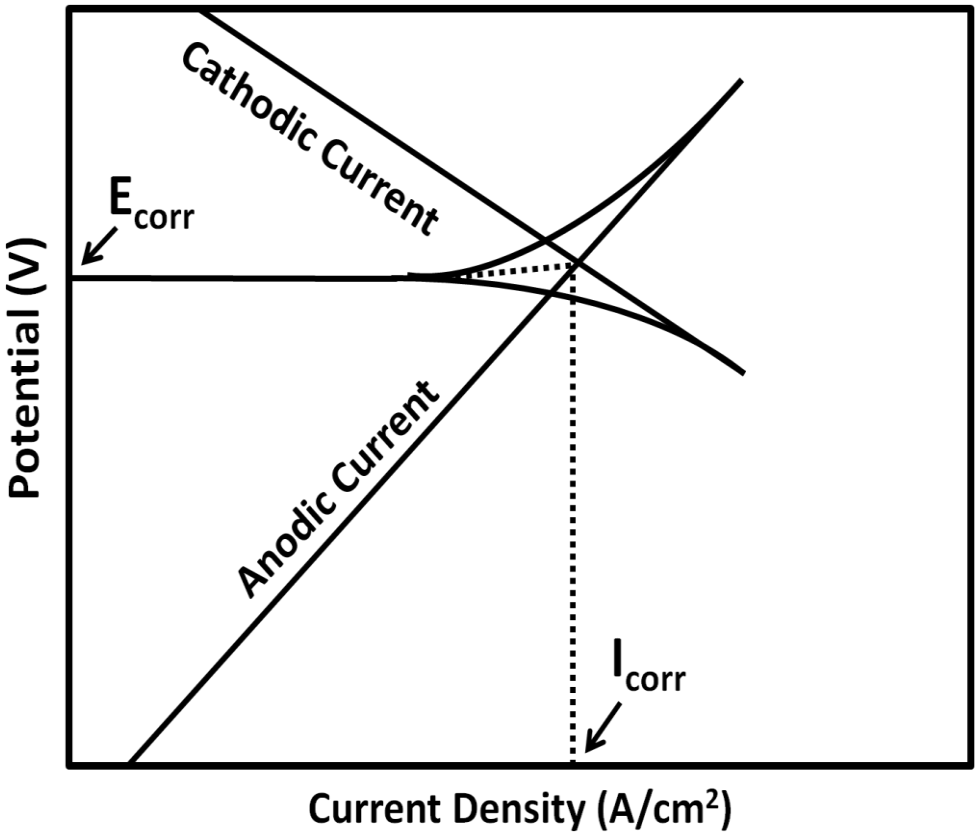

Figure 3.7. Plot of current density against potential

`

CHAPTER 4

RESULTS AND DISCUSSION

4.1 Substrates

4.1.1 Substrate selection

Magnesium oxide (MgO) was used as a substrate in this work. The reason for choosing MgO as a substrate is its small lattice mismatch with the depositing film (gold and TiN). If there is a lattice mismatch between the film and substrate, strain energy accumulates in the growing film. Formation of islands of film materials results in lowering of the strain energy. Some important parameters of MgO include; color: white, melting point: 2780 °C, lattice constant: 4.20 Å, lattice structure: FCC. Figure 4.1 represents the FCC structure of MgO. Properties of MgO include good refractoriness, corrosion resistance, high thermal conductivity, and low electrical conductivity.

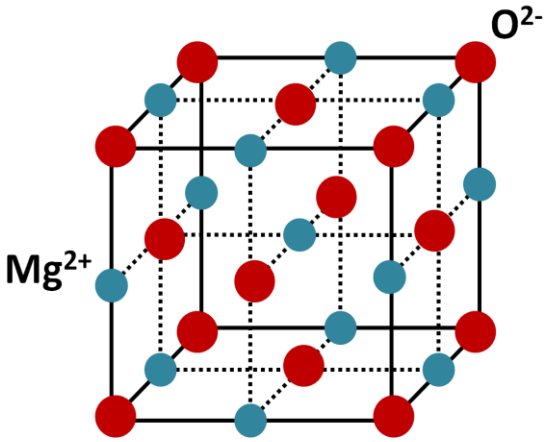

Figure 4.1. Crystal structure of MgO

`

4.1.2 Substrate cleaning

Substrate cleaning is another important step in film deposition experiments. An unclean substrate may introduce contamination, and eventually results in a defective deposition. So it is a very essential to clean the substrate properly before every deposition. First of all, the MgO substrates needed to be cut and placed in a beaker containing acetone. Then the beaker with the substrate was placed in an ultrasonic cleaner for approximately five minutes for sonication. After the ultrasonic cleaning, the beaker with acetone was placed on a heater for vapor cleaning. After the vapor cleaning, the substrate was wiped very gently with acetone.

4.1.3 Substrate surface modification by catalyst

In this work, gold was used as a catalyst. A catalyst is a substance that expedites a chemical reaction, without being consumed by the reaction. Thus, at the end of the reaction, the catalyst can be recovered unchanged. For the nanowire growth, the use of a catalyst is very important. Without catalyst, the deposition becomes a thin film rather than nanowire.

The most commonly-used catalysts for nanowire growth include gold (Au), nickel (Ni) and cobalt (Co). In this work, gold has been chosen as a catalyst due to its small lattice mismatch with substrate (MgO) and nanowire (TiN) materials. Properties of gold include good electrical and thermal conductivity, high melting point etc. It has a face centered cubic (FCC) structure with a lattice constant of 4.14 Å. Figure 4.2 shows the crystal structure of gold.

`

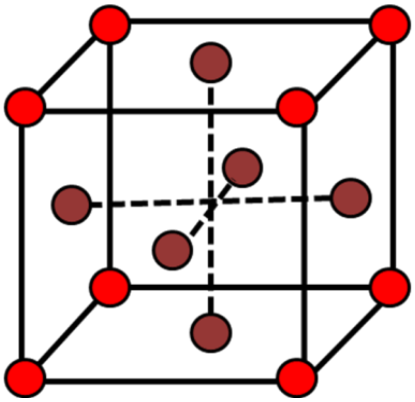

Figure 4.2. Crystal structure of gold

4.2 Thin Film Deposition and Nanowire Fabrication

4.2.1 Growth rate measurement of gold and TiN films

A precise measurement of film thickness is very vital parameter for determining the growth rate of gold and TiN films. To measure the growth rate, a portion of the substrate was covered or masked with a piece of wafer so that the titanium nitride or gold film deposited only on the uncovered part of the substrate surfaces. Once the deposition was completed, thicknesses were measured using a mechanical profilometer. The following growth rates were used in our work: (a) For TiN: 0.016 nm per laser pulse and (b) For gold: 0.024 nm per laser pulse.

4.2.2 Process to grow nanowires

In this work, pulsed laser deposition technique was used for titanium nitride (TiN) nanowire growth. TiN nanowires were grown on magnesium oxide (MgO) single crystal substrates. Prior to the deposition of TiN, the clusters of catalyst (gold) were deposited on the substrate (MgO). A schematic diagram of the TiN nanowire growth process is shown

in Figure 4.3. The thickness of gold catalysts was maintained from 1 to 5 nm by controlling the deposition time (or number of laser pulses). Most of the time, gold was deposited in vacuum and TiN in nitrogen (N_2) environment. A vacuum chamber is a rigid area, where a vacuum pump is used to remove air and other gases. The purpose of the vacuum is to avoid any reaction of the depositing material with any gases present in the air. It protects the sample from any sort of chemical degradation. Both the targets were pre-ablated for 2-3 minutes to clean their surfaces. The pressure in the chamber during gold deposition was of the order of 10^{-6} torr.

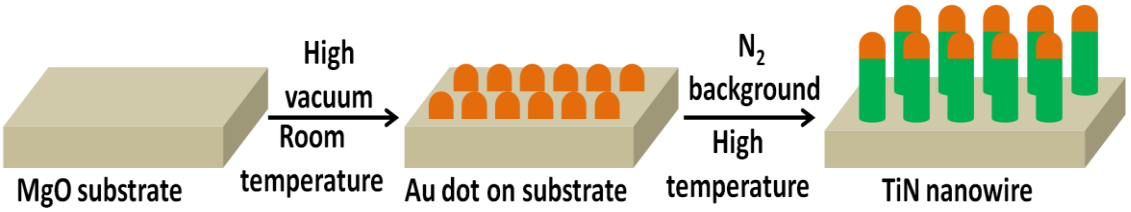

Figure 4.3. Step by step procedure to grow TiN nanowires

A KrF excimer laser [wavelength (λ) = 248 nm, time duration (τ) = 30 ns] operating at a pulse rate of 10 Hz was used for laser ablation. Before the laser ablation of TiN, the gold-coated MgO substrate was preheated at the desired growth temperature for twenty minutes. The growth temperatures were ranged from 600-800 °C. Then TiN was deposited on the substrate at a background pressure of 3×10^{-1} torr of N_2. The deposition time for TiN was varied from 20-30 minutes. Throughout the deposition, the distance between target and substrate was kept at 30 mm. During the nanowire growth, the gold seed remains on top of the nanowires. In many applications we need to remove these gold

dots. But the process to remove the gold tip is still not well developed [49, 50]. After the deposition, the samples were cooled down to room temperature and removed from the PLD chamber for further characterization.

4.3 Structural Properties

4.3.1 Effect of number of laser pulses on gold target in cluster formation

The presence of gold has a significant effect on nanowire growth. Nanowires can grow only on gold clusters, so determining the number of pulses required to form gold clusters of optimum size is very important. For nanowire growth, gold size should be limited to 1-5 nm. To see the effect of gold size, gold films were deposited on MgO substrates using 50, 100, and 500 number of laser pulses. After the deposition, all these gold coated samples were heat treated to 800 °C for twenty minutes. Figure 4.4 shows the SEM image of gold structure on an MgO substrate prepared using different number of laser pulses. In Figure 4.4 (a), the gold film cannot be seen (prepared using 50 laser pulses). The absence of gold film may be attributed to the formation of unstable nuclei or clusters by such a small number of laser pulses. In Figure 4.4 (b), which corresponds to 100 pulses of gold, a well-organized gold cluster can be observed throughout the substrate. In Figure 4.4 (c) a thin film of gold can be clearly seen. In this case, the number of pulses was too high (500) for gold to segregate fully to form gold clusters. Depositing 100 pulses of gold is clearly the best choice for growing gold cluster (dot) and hence for the growth of nanowires.

`

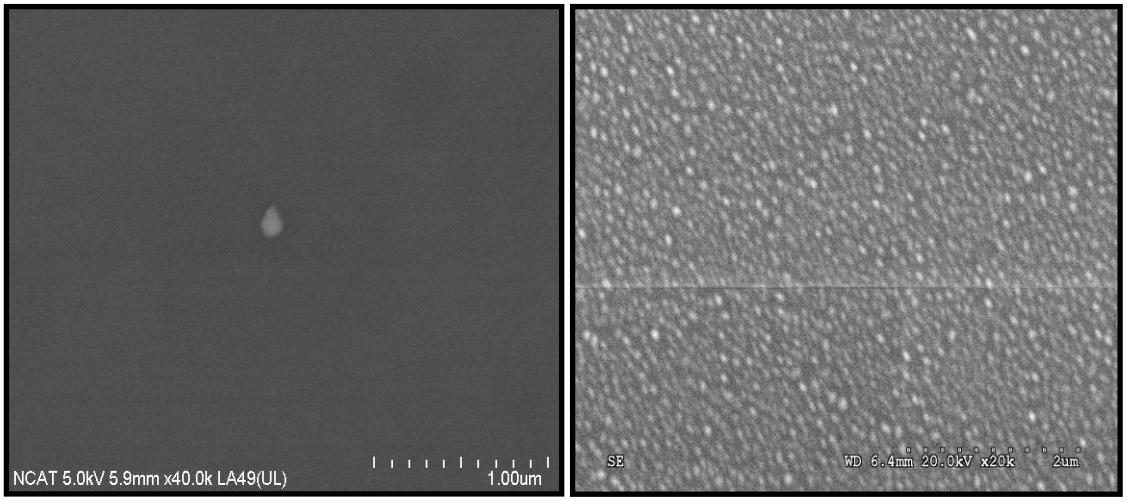

(a) (b)

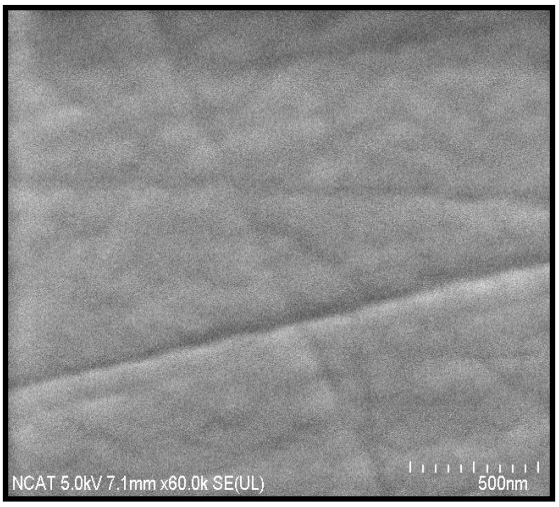

(c)

Figure 4.4. SEM images of gold on MgO substrate with varying number of pulses (a) 50 pulses, (b) 100 pulses, and (c) 500 pulses

`

4.3.2 Effect of deposition temperature on TiN nanowire growth

The deposition temperature has a strong influence on nanowire growth. To see the effect of temperature, gold was deposited on the MgO substrate using 100 number of laser pulses. After the deposition, the temperature of the gold-coated substrates was raised to 400, 600, and 800 °C. Once the required temperature was achieved, 12,000 pulses of titanium nitride (TiN) were deposited on the substrates to grow TiN nanowires. During the deposition the pressure inside the PLD chamber was maintained at 3×10^{-1} torr of N_2.

After the deposition, these three samples made with different deposition temperatures were studied by scanning electron microscope (SEM). After careful observation it is found that 800 °C is the best deposition temperature for TiN nanowire growth as illustrated in Figure 4.5. In Figures 4.5 (a) and 4.5 (b), very few nanowires, scattered on the substrate, can be observed. In these two cases, the deposition temperature was 400 and 600 °C respectively. But in Figure 4.5 (c), at 800 °C, well-fabricated nanowires can be clearly seen throughout the substrate.

The reason is that, at low temperature, the deposited gold structures cannot disaggregate properly and remain as a thin film rather than forming gold dots. So at low temperature, they form a film like structure instead of nanowires. But at high temperature, well-organized gold clusters form, as shown in figure 4.4 (b). These gold clusters facilitate titanium nitride (TiN) nanowire growth on magnesium oxide (MgO) substrate as shown in Figure 4.5 (c). So, high temperature deposition is essential for nanowire growth.

`

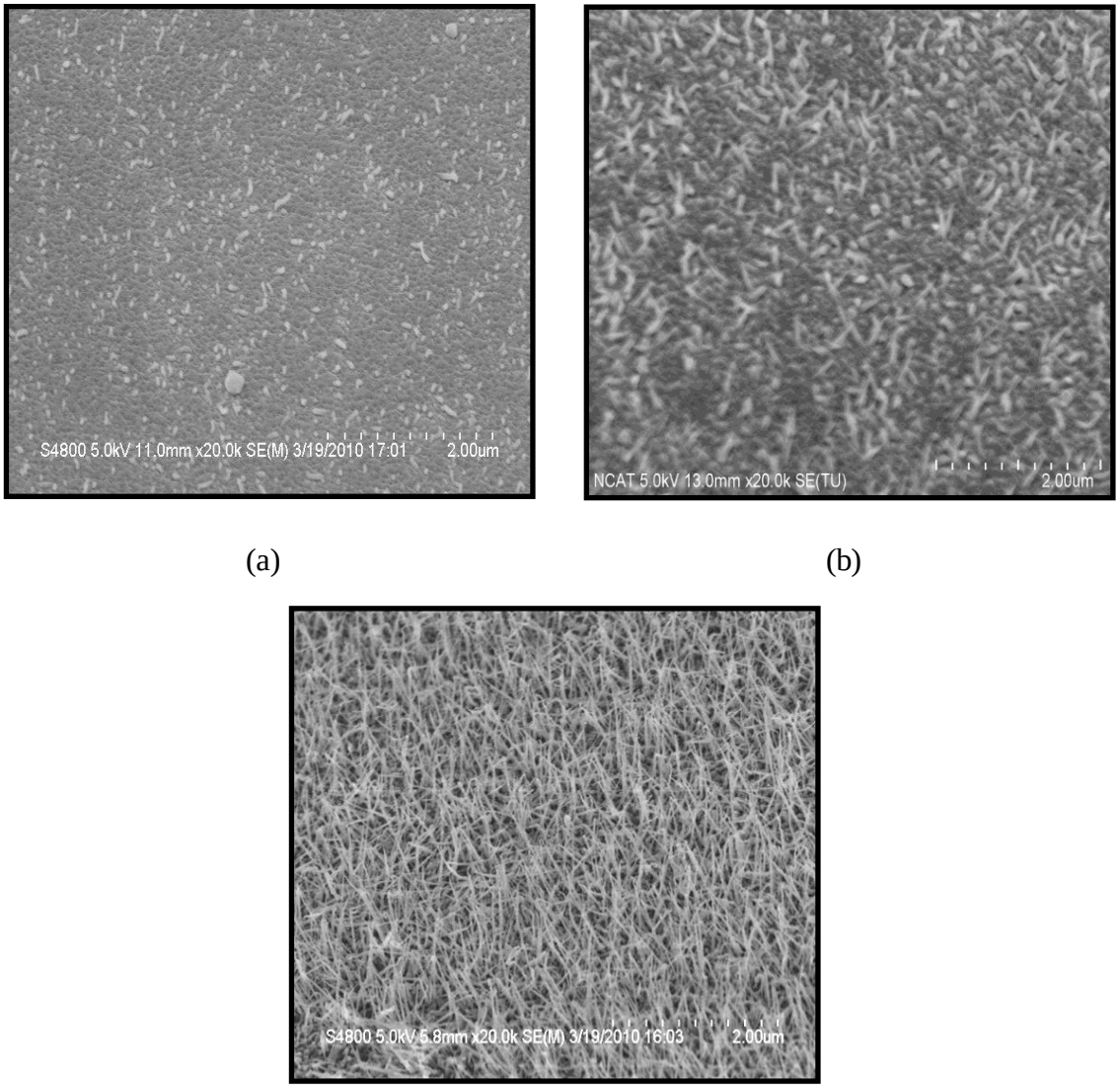

(a) (b)

(c)

Figure 4.5. SEM images with varying deposition temperature (a) 400 °C, (b) 600 °C, and (c) 800 °C

`

Energy dispersive X-ray spectroscopy (EDX) was used to confirm the composition of TiN nanowires. An energy dispersive X-ray spectroscopy (EDX) is a chemical micro-analysis technique normally integrated with SEM. The EDX system consists of an X-ray detector, a liquid nitrogen Dewar, and software to analyze data. The EDX mechanism perceives the X-ray emitted from the sample by an electron beam to characterize the composition of the material. Figure 4.6 shows the EDX data of TiN nanowires, which confirms the presence of TiN and gold (Au) on the MgO substrate.

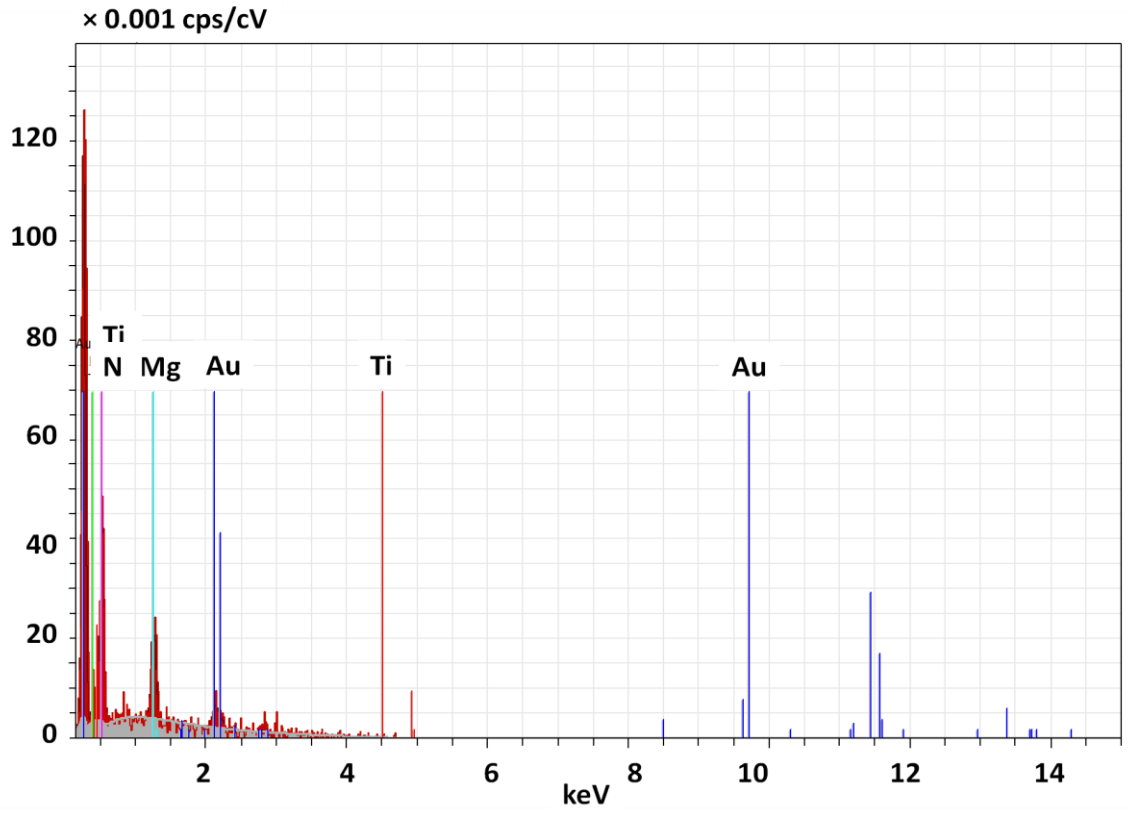

Figure 4.6. Energy dispersive spectroscopy graph of TiN nanowires

`

An experiment has been carried out to demonstrate the fact that nanowire cannot grow without a catalyst. For proving this, a part of the MgO substrate was masked with a silicon wafer and mounted on the PLD chamber. After creating the vacuum in the PLD chamber, 100 pulses of gold were deposited on this masked substrate. Following the deposition the mask was removed from the substrate. So now the substrate has a part with no gold nanodots on it. The substrate was mounted back in the chamber. After raising the temperature to 800 °C, TiN was deposited using 12,000 laser pulses on both parts of the substrate. The corresponding SEM image is shown in Figure 4.7, which confirms that TiN nanowire is grown only on the regions with gold nanodots. The portion of the substrate without gold nanodots produces a thin film of TiN rather than nanowires.

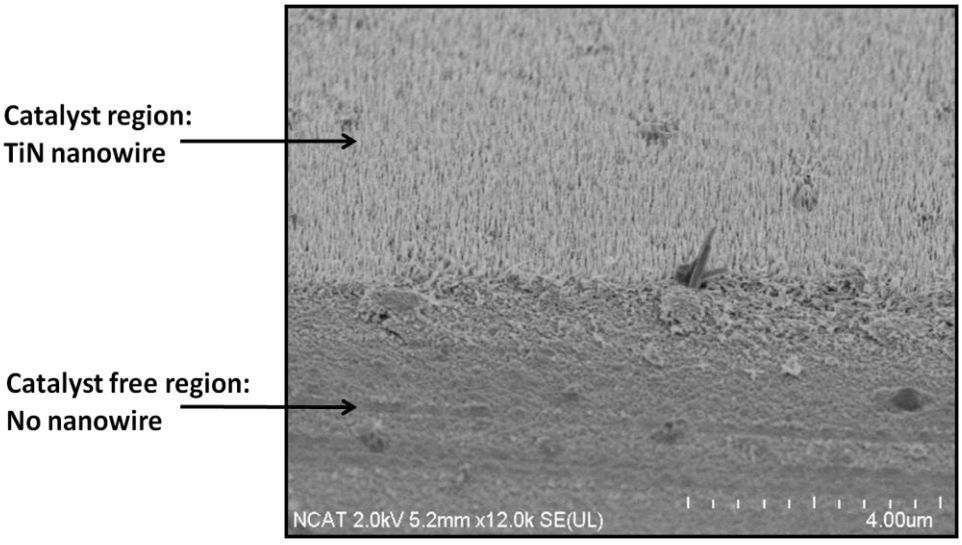

Figure 4.7. SEM image to confirm the dependency of nanowire growth on gold

`

4.3.3 Effect of background gas on TiN nanowire growth

The use of background gas is also very important for nanowire growth. To investigate the effect of background gas, titanium nitride (TiN) was deposited in three different conditions such as vacuum, argon (Ar) and in nitrogen (N_2) environment. Throughout the experiment, the number of laser pulses for gold was kept constant at 100 and deposition temperature was maintained at 800 °C. The surface morphology of these three samples was investigated using scanning electron microscope after the deposition. The corresponding SEM images are shown in Figure 4.8.

Figure 4.8 (a) represents the deposition of TiN in vacuum conditions. It is clear from the figure that the deposition of TiN in vacuum is not suitable for nanowire growth. The deposition in vacuum creates a thin film of TiN rather than nanowires. In Figure 4.8 (b), which corresponds to the deposition of TiN in an argon (Ar) environment, a change in structure of the deposited film can be observed, but still, no nanowire is observed. On the other hand, when TiN was deposited in an N_2 environment, good quality nanowires fabricated throughout the substrate can be clearly seen in Figure 4.8 (c).

So, depositing TiN in N_2 as a background gas is clearly the best option for TiN nanowire growth. We have not observed any nanowires in other two conditions (vacuum and Argon). The use of background gas is vital because it reduces the kinetic energy of the plasma plume, which will effectively change the film properties. The properties of the deposition can be tuned by changing the kinetic energy. Again, the introduction of background gas in PLD can promote surface reaction and maintain film stoichiometry. So, the use of nitrogen as a background gas is very essential for TiN nanowire growth.

`

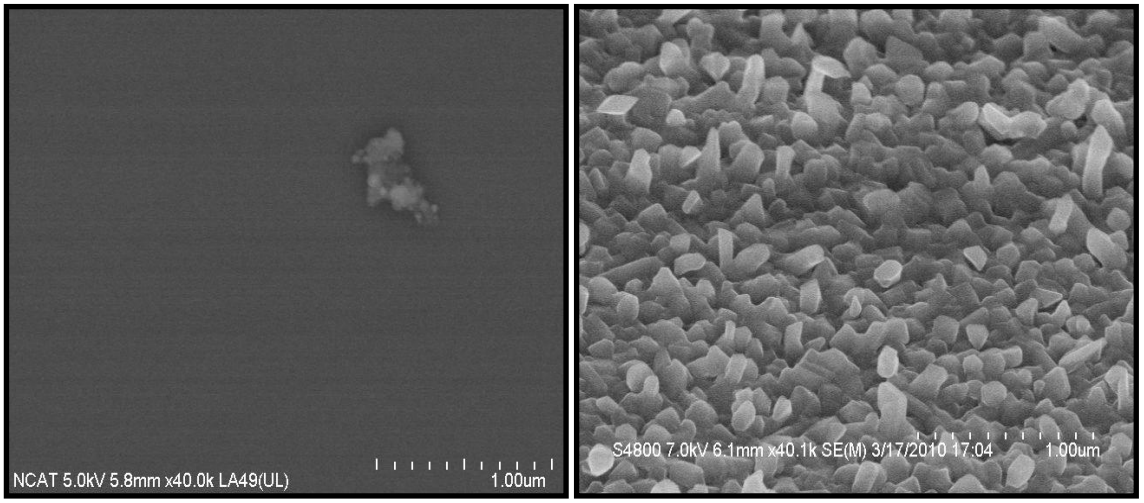

(a) (b)

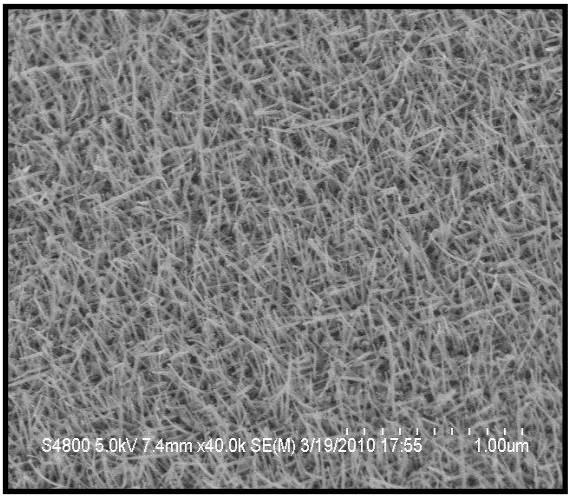

(c)

Figure 4.8. SEM image of TiN nanostructures grown in (a) vacuum, (b) argon, and (c) nitrogen environment

`

4.3.4 Effect of number of laser pulses of TiN on nanowire length

We have optimized all the basic PLD parameters required for TiN nanowire growth so far. We have also determined the number of pulses of gold, deposition temperature and deposition pressure required for TiN nanowire growth. Now our target is to study the effect of the number of laser pulses of TiN on the length of nanowires. In this experiment, 100 pulses of gold were deposited on the MgO substrate. Then the gold coated substrate was annealed to 800 °C. After 20 minutes of annealing at this high temperature, TiN was deposited to grow TiN nanowires. During the deposition, the background pressure was kept at 3×10^{-1} torr of N_2. Only the number of pulses for TiN was changed to investigate its effect. Figure 4.9 represents the corresponding SEM images for 12,000, 18,000 and 30,000 pulses of TiN respectively. From these images, it can be concluded that the length of the nanowire is directly proportional to the number of pulses of TiN.

(a) (b) (c)

Figure 4.9. SEM images with varying number of pulses for TiN (a) 12,000, (b) 18,000, and (c) 30,000 pulses

`

4.3.5 Effect of substrate orientation on the vertical growth of nanowires

The nanowires have been grown so far are not vertical on the substrate. They have grown randomly in different direction. So, the next objective is to grow these nanowires vertically onto the substrate. It is not necessary to grow the nanowires in a vertical direction for using them as a coating material. But it is important to grow nanowires in some controlled direction for using in electronic devices or biosensors.

It is found that the substrate orientation has a substantial impact on the physical, optical and electrical properties of the deposited film. To see the effect of growth direction of TiN nanowires on the orientation of the substrate, TiN was deposited on three different substrates such as MgO (100), MgO (110) and MgO (111). In all three cases, the number of laser pulses for gold was kept constant at 100. After the deposition, this gold coated substrates were raised to 800 °C for annealing. After annealing, 12,000 pulses of TiN were deposited in nitrogen (N_2) environment to fabricate nanowires.

The corresponding SEM images of TiN nanowire for different substrate orientations are shown in Figure 4.10. From the morphology of these three different samples, it is found that on MgO (100) substrate, the nanowires grow randomly throughout the substrate. On MgO (110) substrate, there is a little improvement in verticality. But the nanowires grow vertically only on MgO (111) substrate. So it can be concluded that the growth direction of TiN nanowires is strongly affected by the orientation of the substrate. Figure 4.11 represents the X-ray diffraction (XRD) patterns of MgO (100), MgO (110) and MgO (111) substrate respectively.

`

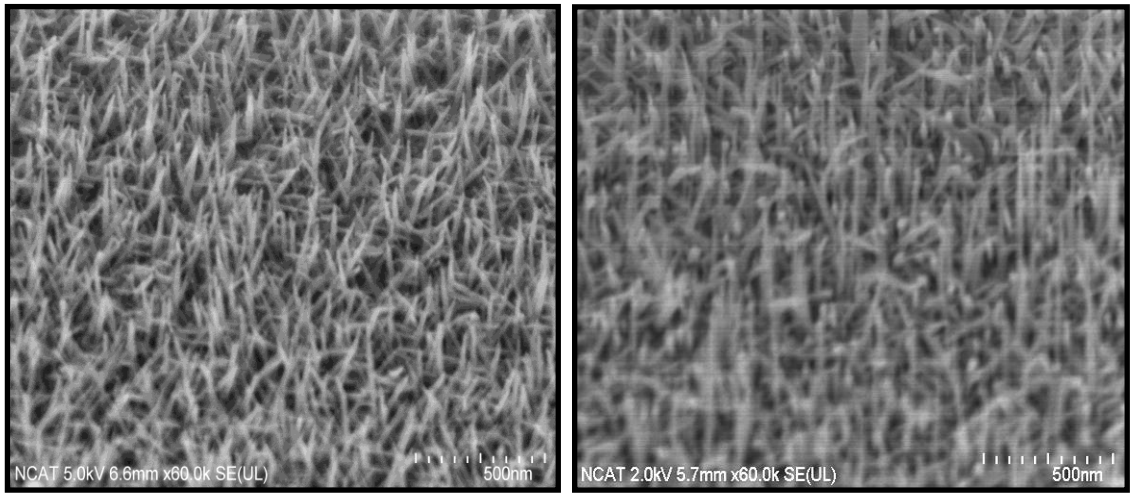

(a) (b)

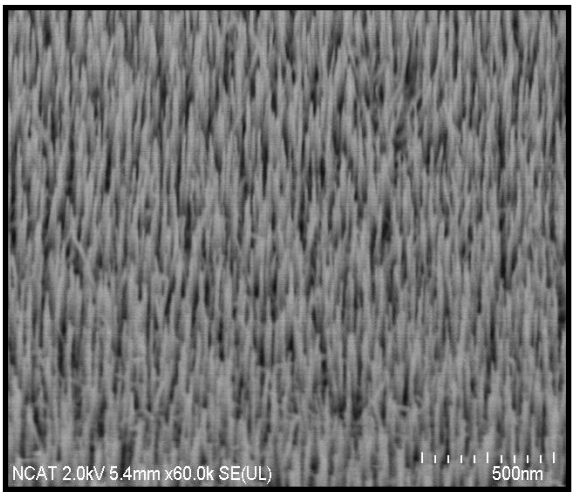

(c)

Figure 4.10. SEM images of TiN nanowire on different orientation of substrate (a) MgO (100), (b) MgO (110), and (c) MgO (111) substrate

`

(a) (b)

(c)

Figure 4.11. X-ray diffraction (XRD) θ-2θ scans of (a) MgO (100), (b) MgO (110), and (c) MgO (111) substrate

`

The crystal structure of all the samples from Figure 4.10 (a-c) was examined using the XRD technique. The details of XRD spectrum of TiN nanowires on three different MgO substrates is shown in Figure 4.12. The XRD spectra have not exhibited any changes in structure with the change in the substrate orientation. In all three cases, cubic structure of TiN with (111) and (222) peaks can be observed. In Figure 4.12 (c) as the orientation of TiN nanowires perfectly coincides with the orientation of MgO (111) substrate, TiN nanowires have grown vertically on MgO (111) substrate. Again, the intensity of the TiN peak on MgO (111) substrate is higher than for the MgO (100) and MgO (110) substrates, which also influence the vertical growth of TiN nanowire on MgO (111) substrate. On other two substrates, TiN has grown in random directions on the substrates. The orientation of the nanowires is highly dependent on the orientation of the substrate and the crystallinity of the peak of the deposition material.

4.3.6 Tapering effect in nanowires

It is important to grow the nanowires uniformly throughout their length. A non-uniformity in nanowire-diameter along their length leads to a tapering effect. In a tapered nanowire, there is the likelihood of developing stress at the top of the nanowire which might result in failure of nanowire. So it is important to reduce the tapering effect from the nanowires. For good quality nanowire growth, the deposition temperature should be higher. But high temperatures lead to the sidewall oxidation of the nanowires, which creates tapering. This sidewall oxidation from the nanowires can be significantly lowered by reducing the temperature.

`

(a) (b)

(c)

Figure 4.12. X-ray diffraction (XRD) θ-2θ scans of TiN nanowire on (a) MgO (100), (b) MgO (110), and (c) MgO (111) substrate

`

But a low temperature deposition can decrease the nucleation density, which results in poor quality nanowire growth. To prevail over this conflicting effect of growth temperature, a two-step procedure was introduced. Under this procedure, the deposition of TiN was started at high temperature (800 °C) and then the temperature was reduced to 600 °C for the rest of the growth period. This procedure does not compromise the quality of nanowires, because high temperature is required only for the initial growth of nanowires. Once they have started forming the temperature can be reduced to eliminate or reduce the tapering effect significantly.

This temperature step during the growth of nanowire helps to reduce the tapering as shown in Figure 4.13. In Figure 4.13 (a), when the entire deposition was performed at 800 °C, some tapering effect on nanowires can be observed. This tapering effect from nanowires is reduced by introducing two-step deposition technique as illustrated in Figure 4.13 (b). To determine the time at which the temperature should be reduced is also very important for reducing the tapering. Figure 4.14 shows the effect when the temperature was reduced to 600 °C after one minute against three minutes. It is found that one minute deposition at high temperature is not adequate for the nanowire nucleation to initiate. In this case, nanowires cannot be seen on the substrate. But when the deposition temperature was reduced to 600 °C after 3 minutes, good quality non-tapered nanowires can be observed. So a better choice is to reduce the temperature to 600 °C after 3 minutes to decrease the tapering effect. From the SEM image, it is obvious that reducing temperature after a fixed time during nanowire growth reduces the tapering and makes the nanowire more cylindrical.

`

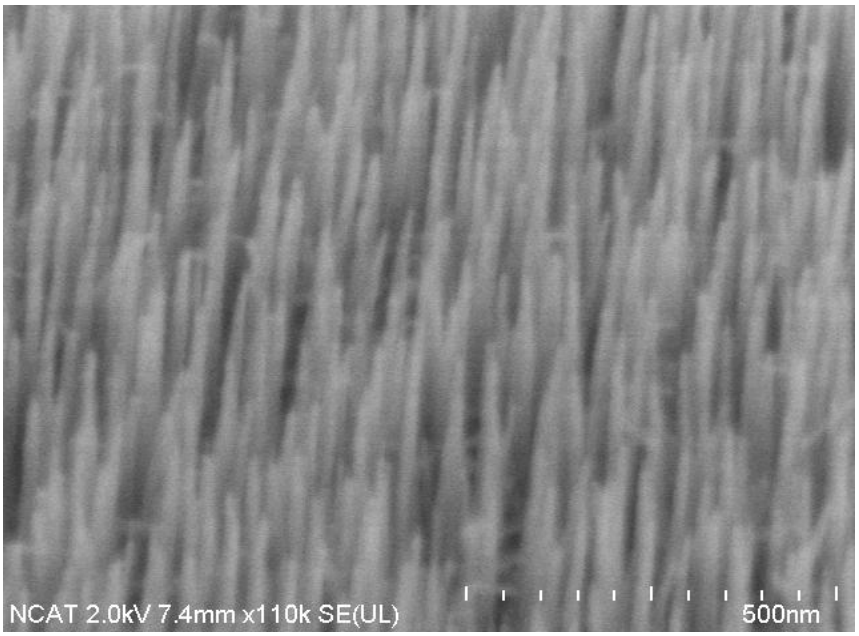

(a)

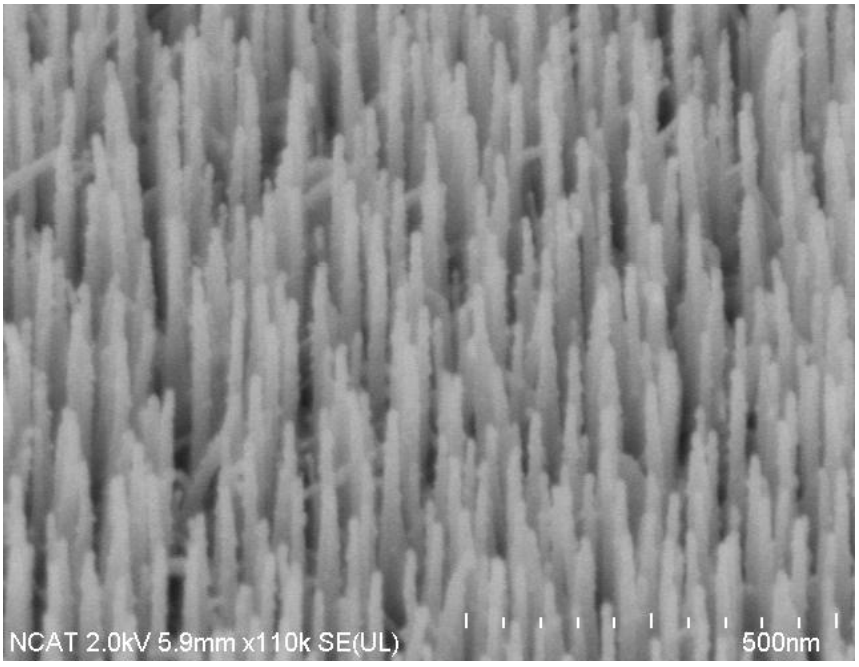

(b)

Figure 4.13. The effect of temperature for reducing tapering of TiN nanowire (a) entire deposition at 800 °C and (b) started deposition at 800 °C (3 minutes) then reduced to 600 °C (15 minutes)

`

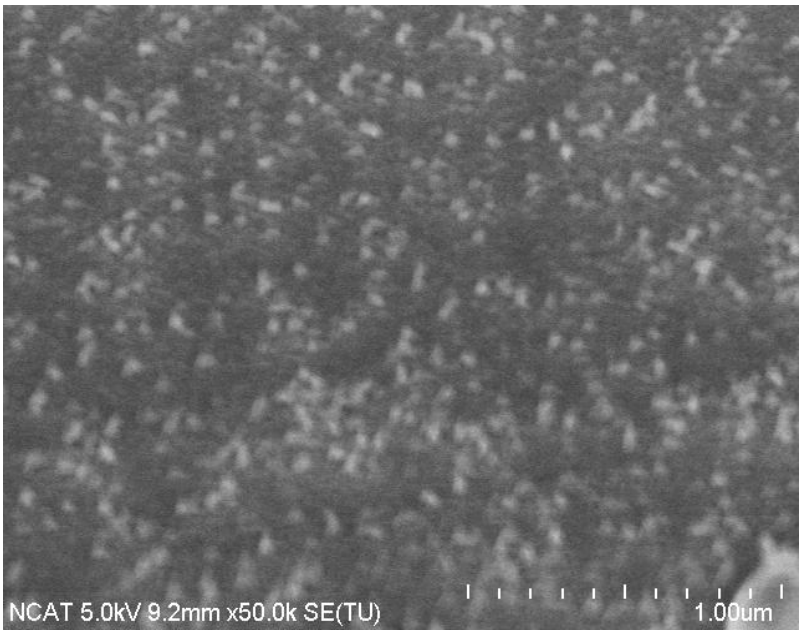

(a)

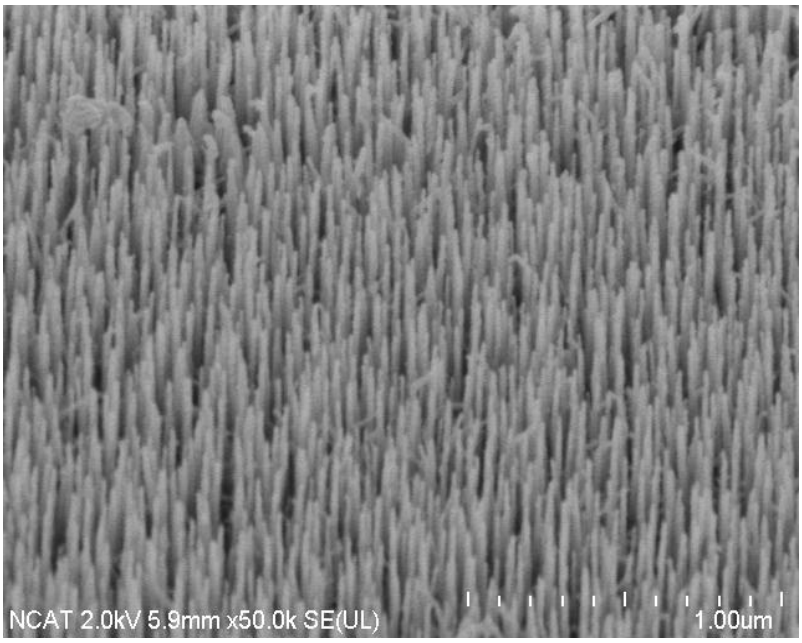

(b)

Figure 4.14. The effect of time for reducing tapering of TiN nanowire by reducing the temperature to 600 °C after (a) 1 minute and (b) 3 minutes

`

4.4 Corrosion and Biological Properties

4.4.1 Corrosion of nanowire

The study of corrosion in the TiN samples is also very important. It improves understanding of the mechanism and basis of corrosion, which helps us to avoid them from occurring. Corrosion can be described as the destruction of metal due to a reaction with the environment. For metals, the corrosion process is mainly electrochemical; the sum of an oxidation and a reduction reaction. To measure corrosion using an electrochemical procedure, the sample should be conductive. As the TiN nanowires grown on MgO substrate are not continuous, there is a gap between adjacent nanowires; current cannot pass through these nanowires. So direct current electrochemical corrosion testing is not possible on these nanowires. But corrosion measurement for TiN thin films is easily accessible. The corrosion testing of TiN thin film has been carried out to obtain a preliminary insight into the corrosion characteristics of the material (TiN).

A thin film of Titanium nitride (TiN) was deposited on an MgO (100) substrate. Prior to the deposition, high temperature annealing was carried out on the substrate. This results in better stoichiometry and crystallinity of the depositing film. Once the temperature was reached the annealing temperature (800 °C), 12,000 pulses of TiN were deposited on the annealed MgO substrate. During the deposition, the pressure inside the chamber was kept approximately at 10^{-7} torr.

After the deposition, the crystal structure of the TiN thin films was investigated using X-ray diffraction (XRD) technique. The XRD spectrum of a TiN thin film on an MgO (100) substrate using Cu K_α radiation with X- ray energy about 8 eV is shown in

`

Figure 4.15. X- ray diffraction data confirms the presence of a face centered cubic (FCC) TiN structure with (111) and (222) diffraction peaks. The morphology of the TiN thin film and Mg substrate is shown in Figure 4.16. Figure 4.16 (a) and 4.16 (b) represents the SEM images of the TiN thin film before and after the corrosion test. Before conducting the corrosion test, the TiN thin film samples were immersed in the Hank's balanced salt solution (HBSS) and phosphate buffer saline (PBS) solution for 48 hours. Some initiation of corrosion in TiN thin film can be observed after the corrosion test, as shown in Figure 4.16 (b). The corrosion in the TiN thin film is not severe compare to the corrosion effect in the Mg substrate, as shown in Figure 4.16 (d).

Figure 4.15. X-ray diffraction (XRD) θ-2θ scans of TiN thin film on MgO (100) substrate

`

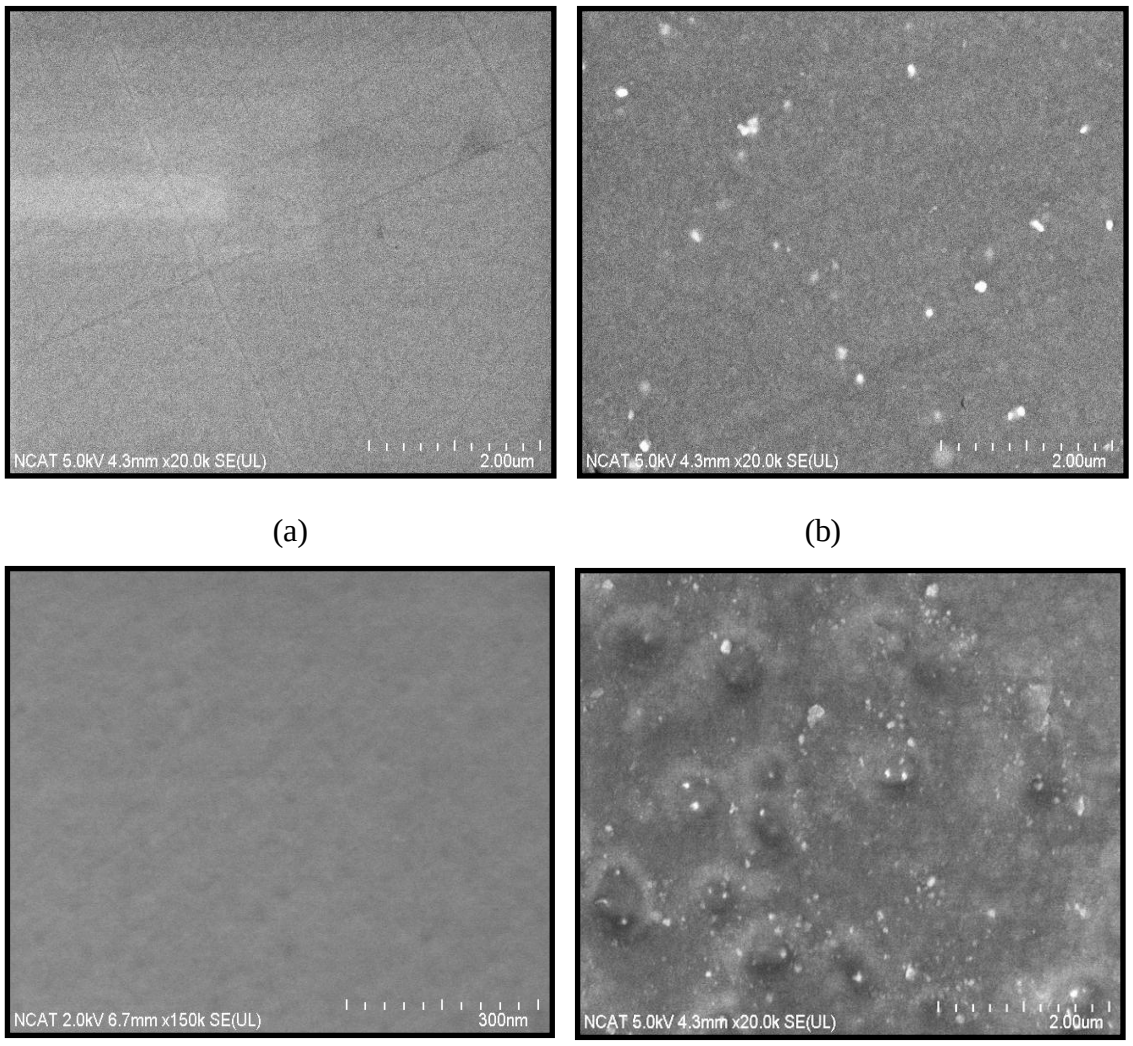

Figure 4.16. SEM images of (a) TiN thin film before corrosion test, (b) TiN thin film after corrosion test, (c) Mg substrate before corrosion test, and (d) Mg substrate after corrosion test

`

The setup for corrosion testing includes a reference and a counter-electrode, an electrolyte solution, and the sample which is also known as the working electrode. All the electrodes were connected to a potentiostat and placed in the electrolyte solution. In the experiment two types of solution were used, hanks balanced salt solution (HBSS) solution and phosphate buffer saline (PBS) solution. Both of these solutions simulate body fluid. The pH value for HBSS solution ranges from 7.14-7.46 and pH value for PBS solution varies from 7.3-7.5. After connecting the sample to the potentiostat, a voltage was applied to the electrodes. In the process, the applied potential was increased with time and the corresponding current was measured. From the energy difference between the working and reference electrodes, the corrosion potential was measured. Then the current density was plotted against the potential. This procedure was repeated after 48 hours. During these 48 hours, the samples were immersed in the solution. The corresponding potentiodynamic polarization graphs of TiN thin film for both cases (initial and after 48 hours) and the Mg substrate are shown in Figure 4.17.

Figure 4.17 (a) and 4.17 (b) represent the corrosion results of TiN thin film and Mg substrate in HBSS and PBS solution respectively. From the polarization graph, the corrosion current (I_{corr}) and corrosion potential (E_{corr}) can be deduced. The intersection of the slope of anodic and cathodic current provides I_{corr} and E_{corr}. The x-axis of this intersection point gives the corrosion current and corresponding y-axis represents corrosion potential. A lower value of I_{corr} signifies higher corrosion resistance and higher E_{corr} indicates higher corrosion resistance.

`

(a)

(b)

Figure 4.17. Potentiodynamic polarization curve of TiN thin film in (a) HBSS solution and (b) PBS solution

`

The corrosion potential (E_{corr}) and corrosion current (I_{corr}) data deduced from these two potentiodynamic polarization graphs are shown in Table 4.1 and 4.2. It can be clearly seen from these two tables that, TiN thin film, before and after 48 hours of immersion in solutions like HBSS and PBS exhibits lower I_{corr} and higher E_{corr} than Mg substrate. From this data, it can be concluded that TiN thin film possesses better corrosion characteristics than Mg substrate. TiN thin film, as they acquire good corrosion resistance than commonly used implant materials can be used as a coating material in biological field, especially in bio-stable applications like stents, pacemakers, heart valves, orthopedics etc.

Table 4.1. Corrosion potential and corrosion current data for TiN thin film and Mg substrate in HBSS solution

Sample	I_{corr} (A/cm^2)	E_{corr} (V)
TiN	2.6×10^{-6}	-0.32
TiN after 48 hours	1.5×10^{-5}	-0.68
Mg	7.7×10^{-4}	-1.4

Table 4.2. Corrosion potential and corrosion current data for TiN thin film and Mg substrate in PBS solution

Sample	I_{corr} (A/cm^2)	E_{corr} (V)
TiN	1.6×10^{-5}	-0.33
TiN after 48 hours	3.3×10^{-5}	-0.65
Mg	1.7×10^{-4}	-1.2

`

4.4.2 Cell culture

4.4.2.1 Objective

As the human body has natural resistance to foreign materials, it is difficult for implant materials to be adapted into the body. Most implants today are made from either titanium-based alloys or alloys made from a mixture of cobalt and chromium. Both of them exhibit superior mechanical properties, but neither is able to bond with bone. As a consequence, these metals may rub against the bones into which they have been implanted, creating wear and tear that shortens implant lifetimes. There is thus a huge demand for new coating materials like TiN nanowires which can stick well to the metal surface of implants and should also encourage bone formation. In order to use these nanowires as coating materials, it is very important to check their biocompatibility to ensure that cells can survive and grow around these nanowires. An effective tissue culture can generate lots of results, such as observation and study of pathogenesis (progress of disease), study of cell damage, repair and apoptosis (cell death), and analysis of drug delivery mechanisms.

4.4.2.2 Aseptic technique

About 70 % of the problems during a tissue culture test are associated a lack of good sterile technique. The aseptic technique acquires a cell culture test by avoiding any sort of contamination from the environment. A comprehensive effort is required to maintain a sterile environment. All the pipettes, glass-ware and solutions must be sterilized by autoclaving. For sterilizing the medium, it should be passed through a filter. The filter must be small enough to block bacteria and mycroplasmas.

`

During cell culture experiments, one should be very careful about all sort of contamination. Contamination may arise from numerous sources like bacteria, fungi, and viruses etc. Before commencing any work, all the cabinets, materials, flasks, tubes, and equipment must be sanitized with 70 % ethanol. A sterile flask, bottle or Petri dish should not be uncovered until ready to use. All the flasks, bottles or wells must be covered immediately after work. None of these accessories can be left open to the environment, it may results in contamination. The same pipette should not be used in different bottles as there is a huge probability of cross contamination. A sterile pipette should be used for each operation, especially for pipetting medium. All the liquid waste and pipettes should be disposed safely after experiment. Even talking, sneezing or coughing during experiment can cause contamination. So prudence is the most important criterion in cell culture research.

4.4.2.3 Accessories

A laminar flow hood is used to maintain a contamination-free environment for the cell culture test. In a hood, the air passes through a high efficiency particle filter which can eliminate particulates from the air. This hood normally equipped with a UV light which can be turned on for a few minutes to sterilize the hood. The exposed area of the hood should be cleaned by ethanol before and after every use. For the cell growth, a nontoxic, biologically static, and optically transparent surface is required that can facilitate cell growth. A sterile vessel should be used, which can be disposable. Most commonly used vessels include Petri dishes, multi-well plates, flasks etc.

`

4.4.2.4 Cell growth

Human and animal cells can be customized to grow *in vitro* on plastic flasks, glass slides or in wells. The primary task is to select the cell of interest based on the application. We have used osteoblast cells to perform tissue culture tests, as our research is related to bone implant. Osteoblasts are cells responsible for bone formation. After selecting the cell line, the next step is to select an appropriate medium which can enhance cell growth by providing the proper environment, nutrient and maintaining the proper pH. In the experiment, Dulbecco's modified eagle medium (DMEM) was used as a medium. To enhance the performance of the medium, 50 ml of fetal bovine serum (FBS), 500 µl of Genetycin (antibacterial) and 500 µl of nystatin (antifungal) was added to the 500 ml of DMEM. For the cell suspension, 9 ml of DMEM media was added to 1 ml of cell. After preparing the cell suspension, 9 ml of media was added to 1 ml of cell suspension in a T-75 flask. For the cell proliferation, this flask was kept in a CO_2 incubator. After two days, the flask was observed under an inverted microscope to see the growth rate. It was found that the bottom surface of the flask was covered almost 50 % by the cells. For more proliferation 5 ml of new media was added in the flask. When the flask surface reaches 80 % of its confluence the cells were divided into two different flasks for more proliferation. Before splitting, all the old media from the flask were aspirated. Then 4 ml of trypsin was added to the flask to detach the cells from the bottom of the flask. After that, 20 ml of media was added to the flask. This 24 ml of solution was divided into two new flasks for further proliferation of cells. These two flasks were then kept in the CO_2 incubator. After 96 hours, they were ready to use on the samples.

`

4.4.2.5 Lactate dehydrogenase (LDH) release assay

Lactate dehydrogenase (LDH) assay is a fast, accurate and simple process to quantify cytotoxicity. This method measures cytotoxicity by counting the amount of LDH activity released by damaged cells. The higher the LDH release, the higher the toxicity. The LDH assay is executed in a 96-well microplate. LDH can be used to observe a variety of *in vitro* cells, where damage to the plasma membrane happens. It can determine the cytotoxicity of compounds in food, cosmetics industry and medical research. Mediator-induced cytolysis can also be determined by LDH. Cell death in bioreactors can also be determined using this method.

There are three different controls used in an LDH assay. Background control is used to calculate the LDH activity contained in the assay medium. Low control decides the LDH activity discharged from the untreated cells and high control determines the highest releasable LDH activity in the cells. Lactate dehydrogenase (LDH) is a cytoplasmic enzyme. LDH is present in all mammalian cells. There is a likelihood of plasma membrane damage when the cells come in contact with toxic substances or substrates. As a result, LDH leaks into surrounding media. A colorimetric assay is used to detect LDH activity released from the cytosol of the cells that have incurred plasma membrane and hence determine the LDH level.

In this work, osteoblast cells were seeded onto the substrates and TiN nanowires at a density of 5×10^5 cells per well. 500 µl of media was added to the samples during certain time points (4 hours and 24 hours) to evaluate the concentration of LDH release using LDH cytotoxicity detection kit. A 96-well microplate was used for performing the

LDH test, the experimental media (in triplicate) along with high and low controls was analyzed on micro devices spectrophotometer plate reader at a wavelength of 488 nm. The corresponding histograms for LDH released assay after 4 hours and 24 hours on different controls and nanowires sample are shown in Figure 4.18. The higher value of LDH release indicates higher toxicity. From both histograms (4 hours and 24 hours), it can be seen that the LDH release from all the nanowire samples are close to the LDH release from the low control and way lower than high control. This low LDH release from the samples indicates the low cytotoxicity of TiN nanowires. It can be concluded from these cytotoxicity tests that these TiN nanowires are biocompatible and are suitable candidate materials for using as a coating in biomedical implants or in other biological applications.

`

(a)

(b)

Figure 4.18. LDH release assay after (a) 4 hours and (b) 24 hours

`

CHAPTER 5

CONCLUSIONS AND FUTURE WORK

5.1 Conclusions

The objective of this work was to fabricate titanium nitride nanowires and characterize their physical, structural, and biological properties. The effect of gold nanodots, nature and pressure of background gas, and the deposition temperature on the growth of TiN nanowires was investigated in this study. The gold cluster prepared by 100 number of laser pulses using gold target was found to be best suited for nanowire formation. It was also found that, deposition temperature and pressure have substantial effects on the growth of TiN nanowires. Deposition of TiN on the gold-coated substrate at high temperature (800 °C) and appropriate background condition (3×10^{-1} torr of N_2) results in TiN nanowires formation with the best quality. It was also confirmed that the vertical growth of these TiN nanowires are highly dependent on the orientation of the substrate. Using this approach, TiN nanowires were found to grow vertically on the MgO (111) substrate. The significance of deposition temperature on reducing the tapering effect from TiN nanowires was also confirmed in this work. A two-stage deposition technique was used in this study, which includes the starting of deposition of TiN at high temperature (800 °C) and then reducing the temperature to 600 °C after three minutes for the remaining deposition period to reduce the tapering of the nanowires. In addition to the synthesis of nanowires, the corrosion characteristics and biocompatibility of these

`

nanowires were also investigated in this work as our focus is to use these nanowires as coating material for implants inside the body. From the corrosion test, it was confirmed that TiN thin film has better corrosion resistance than magnesium (Mg) substrate. The corrosion characteristic of TiN thin films was measured in two different solutions, hanks balanced salt solution (HBSS) and phosphate buffer saline (PBS) solution. In both the cases, TiN exhibits better corrosion resistance than the Mg substrate. TiN thin films, as they possess better corrosion resistance can be used as a coating material in bio-stable applications like stents, pacemakers, heart valves, orthopedics etc. The cytotoxicity of TiN nanowires was evaluated by LDH release assay. Osteoblast cells were used as the cell line for this test. The LDH release assay confirmed the low toxicity of these nanowires. So, it can be concluded with conviction that titanium nitride (TiN) nanowires have a huge potential in biological application.

5.2 Future Work

The present work has shown that TiN does not corrode appreciably in simulated body fluids such as HBSS, PBS solution. The nanowires have also been found to be biologically non-toxic to osteoblast cells. However, more detailed research is required to be carried out in both the areas of corrosion and cytotoxicity. Since the cells are different in the different regions of the body, it will be worthwhile to investigate the effect of TiN on various cells. The selections of the cells will be made based on the application area. The future work will also involve testing the effect of TiN nanowire coatings on the life and performance of existing implant materials such as magnesium, titanium, and stainless

`

steel. It will also be interesting to apply TiN nanowire coating on magnesium bulk plates and wires and study their corrosion and biological properties.

`

REFERENCES

[1] Wagner, R. S., and Ellis, W. C., 1964, "Vapor-liquid-solid mechanism of single crystal growth," Appl. Phys. Lett., **4**, pp. 89-90.

[2] Xia, Y., Yang, P., Sun, Y., Wu, Y., Mayers, B., Gates, B., Yin, Y., Kim, F., and Yan, H., 2003, "One-dimensional nanostructures: Synthesis, characterization, and applications," Adv. Mater., **15**, pp. 353-389.

[3] Goddard, W.A., 2003, "Handbook of Nanoscience, Engineering, and Technology," CRC Press LLC.

[4] Talyansky, V., Vispute, R. D., Ramesh, R., Sharma, R. P., Venkatesan, R. P., Li, Y. X., Salamanca-Riba, L. G., Wood, M. C., Lareau, R. T., Jones, K. A., and Iliadis, A. A., 1998, "Fabrication and characterization of epitaxial AlN/TiN bilayers on sapphire," Thin Solid Films, **323**, pp. 37-41.

[5] Inumaru, T. O., and Yamanaka, S., 2000, "Pulsed laser deposition of epitaxial titanium nitride on MgO (001) monitored by RHEED oscillation," Appl. Surf. Sci., **158**.

[6] Nishizawa, M., Menon, V. P., and Martin, C. R., 1995, "Metal nanotubule membranes with electrochemically switchable ion-transport selectivity," Science (Washington, D. C.), **268**, pp. 700-2.

[7] Liang, C. H., Chen, L. C., Hwang, L. S., Chen, K. H., Hung, Y. T., and Chen, Y. F., 2002, "Selective-area growth of indium nitride nanowires on gold-patterned Si(100) substrates," Appl. Phys. Lett., **81**, pp. 22-24.

[8] Pan, Z., Lai, H. L., Au, F. C. K., Duan, X., Zhou. W., Shi, W., Wang, N., Lee, C. S., Wong, N. B., Lee, S. T., and Xie, S., 2000, "Oriented silicon carbide nanowires: synthesis and field emission properties," Adv. Mater., **12**, pp. 1186-1190.

[9] Mathur, S., Barth, S., Werner, U., Harnandez, F., and Romano, A., 2008, "Chemical vapor growth of one-dimensional magnetite nanostructures," Adv. Mater., **20**, pp. 1550-1554.

[10] Samuelson, L., 2003, "Self-forming nanoscale devices," Materials Today, **6**, pp. 22-31.

[11] http://www.physorg.com/news106579911.html.

[12] http://science.howstuffworks.com/nanowire1.htm.

[13] Dick, K., Dhanasekaran, T., Zhang, Z., and Meisel, D., 2002, "Size-dependent melting of silica-encapsulated gold nanoparticles," J. Am. Chem. Soc., **124**, pp. 2312-2317.

[14] Chan, C. K., Ruffo, R., Hong, S. S., Huggins, R. A., and Cui, Y., 2009, "Structural and electrochemical study of the reaction of lithium with silicon nanowires," Journal of Power Sources, **189**, pp. 34-39.

[15] http://fuel-efficient-vehicles.org/energy-news/?cat=1.

[16] Duan, X., Huang, Y., Cui, Y., Wang, J., and Lieber, C. M., 2001, "Indiumphosphide nanowires as building blocks for nanoscale electronic and optoelectronic devices," Nature (London), **409**, pp. 66-69.

[17] Huang, Y., Duan, X., Cui, Y., Lauhon, L. J., Kim, K. H., and Lieber, C. M., 2001, "Logic gates and computation from assembled nanowire building blocks," Science, **294**, pp. 1313-7.

[18] Huang, Y., Duan, X., Cui, Y., and Lieber, C. M., 2002, "Gallium Nitride Nanowire Nanodevices," Nano Lett., **2**, pp. 101-104.

[19] Huang, Y., Bai, X., and Zhang, Y., 2006, "In situ mechanical properties of individual ZnO nanowires and the mass measurement of nanoparticles," J. Phys.: Condens. Matter, **18**, pp. L179-L184.

[20] http://newscenter.lbl.gov/feature-stories/2007/08/06/embedded-a-benign-way-to-nanowire-living-cells/.

[21] Chen, Y., Wang, X., Erramilli, S., Mohanty, P., and Kalinowski, A., 2006, "Silicon-based nanoelectronic field-effect pH sensor with local gate control," Appl. Phys. Lett., **89**, pp. 223512/1-223512/3.

[22] Kottke, M., Gregory, R., Pintchovski, F., Travis, E., and Tobin, P.J., 1991, "Auger electron spectroscopy and Rutherford backscattering characterization of titanium nitride/titanium silicide contact barrier metallization," J. Vac. Sci. Technol., **9**, pp. 74-88.

[23] Paschoal, A. L., Vanancio, E. C., Canale, L. C. F., Lopes, S. V., and Huerta, D., 2003, "Metallic biomaterials TiN-coated: corrosion analysis and biocompatibility," Artif. Organs, **27**, pp. 461-464.

`

[24] Lombardi A. V., Vaughn, B. K., and Drouillard, P., 1989, "Aseptic loosening in total hip arthroplasty secondary to osteolysis induced by wear debris from titaniumalloy modular femoral heads," J Bone Joint Surg., **71**.

[25] McDonald, M. D., and Bloebaum, R. D., 1995, "Distinguishing wear and creep in clinically retrieved polyethylene inserts," J Biomed Mater Res., **29**, pp. 1-7.

[26] Kawalec, J. S., and Brown, S. A., 1995, "Fretting corrosion of untreated and nitrided Ti6A14V fretted against bone and bone cement," Trans Soc Biomater., **18**.

[27] http://www.endotec.com/Femoral-Stem-Design-Rationale.htm

[28] Cigada A, B.M.P.D., 1993, "Wear and creep of UHMWPE by hip joint simulator tests," Trans Soc Biomater., **16**.

[29] Peterson, C. D., Hillberry, B. M., and Heck, D. A., 1988, "Component wear of total knee prostheses using Ti-6A1-4V, titanium nitride coated Ti-6A1-4V, and cobalt-chromium-molybdenum femoral components," J Biomed Mater Res., **22**, pp. 887-903.

[30] Muratore, C., Hu, J. J., and Voevodin, A. A., 2007, "Adaptive nanocomposite coatings with a titanium nitride diffusion barrier mask for high-temperature tribological applications," Thin Solid Films, **515**, pp. 3638-3643.

[31] Matenoglou, G. M., Logothetidis, S., and Kassavetis, S., 2006, "Durable TiN/TiNx metallic contacts for solar cells," Thin Solid Films, **511-512**, pp. 453-456.

[32] Manso, M., Ogueta, S., Perez-Rigueiro, J., Garcia, J. P., and Martinez-Duart, J. M., 2002, "Testing biomaterials by the in-situ evaluation of cell response," Biomol. Eng., **19**, pp. 239-242.

[33] Raimondi, M. T., and Pietrabissa, R., 2000, "The in-vivo wear performance of prosthetic femoral heads with titanium nitride coating," Biomaterials, **21**, pp. 907-13.

[34] Carney, C., and Durham, D., 1999, "Establishing the relationship between process, structure, and properties of TiN films deposited by electron cyclotron resonance assisted reactive sputtering. I. Variations in hardness and roughness as a function of process parameters," J. Vac. Sci. Technol., B.

[35] Grigorov, K., Grigorov, G., Stoyanova, M., Vignes, J. L., Langeron, J.P., Denjean, P., and Perriere, J., 1992, "Diffusion of silicon in titanium nitride films: efficiency of titanium mononitride barrier layers," Appl. Phys. A., **A55**, pp. 502-4.

[36] Noel, J. P., Houghton, D. C., Este, G., Shepherd, F. R., and Plattner, H., 1984, "Characteristics of dc magnetron, reactively sputtered titanium nitride (TiNx) films for diffusion barriers in III-V semiconductor metalization," J. Vac. Sci. Technol., A, **2**, pp. 284-7.

[37] http://www.titanium-fiko.com.ua/pages/TiN_e.htm.

[38] Yanagida, T., Nagashima, K., Tanaka, H., and Kawai, T., 2008, "Mechanism of critical catalyst size effect on MgO nanowire growth by pulsed laser deposition," J. Appl. Phys., **104**, pp. 016101/1-016101/3.

[39] Sorensen, C. M., Magnetism. 2001: John Wiley & Sons, Inc.

[40] Nagashima, K., Yanagida, T., Oka, K., Tanaka, H., and Kawai, T., 2008 "Mechanism and control of sidewall growth and catalyst diffusion on oxide nanowire vapor-liquid-solid growth," Appl. Phys. Lett., **93**, pp. 153103/1-153103/3.

[41] Jagannathan, H., Deal, M., Nishi, Y., Woodruff, J., Chidsey, C., and Mclntyre, P.C., 2006, "Nature of germanium nanowire heteroepitaxy on silicon substrates," J. Appl. Phys., **100**, pp. 024318/1-024318/10.

[42] Kim, H. W. and Shim, S. H., 2006, "Growth of MgO nanowires assisted by the annealing treatment of Au-coated substrates," Chem. Phys. Lett., **422**, pp. 165-169.

[43] Nagashima, K., Yanagida, T., Tanaka, H., and Kawai, T., 2007, "Epitaxial growth of MgO nanowires by pulsed laser deposition," J. Appl. Phys., **101**, pp. 124304/1-124304/4.

[44] Wu, J. J., and Liu, S. C., 2002, "Low-temperature growth of well-aligned ZnO nanorods by chemical vapor deposition," Adv. Mater., **14**, pp. 215-218.

[45] Kong, Y. C., Yu, D. P., Zhang, B., Fang, W., and Feng, S. Q., 2001, "Ultraviolet-emitting ZnO nanowires synthesized by a physical vapor deposition approach," Appl. Phys. Lett., **78**, pp. 407-409.

[46] Vayssieres, L., Keis, K., Lindquist, S., and Hagfeldt, H., 2001, "Purpose-built anisotropic metal oxide material: 3D highly oriented microrod array of ZnO," J. phys. Chem., **105**, pp. 3350-3352.

[47] Venkatesan, T., and Green, S. M., 1996, "Pulsed laser deposition: thin films in a flash," Ind. Phys., **2**, pp. 22-24.

[48] Cheung, J. T., "History and fundamentals of pulsed laser deposition," 1994: Wiley.

[49] Kawashima, T., Saitoh, T., Komori, K., and Fujii, M., 2009, "Synthesis of Si nanowires with a thermally oxidized shell and effects of the shell on transistor characteristics," Thin Solid Films, **517**, pp. 4520-4526.

[50] Putnam, M. C., Filler, M. A., Kayes, B. M., Kelzenberg, M. D., Guan, Y., Lewis, N. S., Eiler, J. M., and Atwater, H. A., 2008, "Secondary ion mass spectrometry of vapor-liquid-solid grown Au-Catalyzed, Si Wires," Nano Lett., **8**, pp. 3109-3113.